Journal of Structural Biology 196 (2016) 244–259

Contents lists available at ScienceDirect

Journal of Structural Biology

journal homepage: www.elsevier.com/locate/yjsbi

Nonclassical crystallization *in vivo et in vitro* (I): Process-structure-property relationships of nanogranular biominerals

Stephan E. Wolf [a,b,*], Corinna F. Böhm [a], Joe Harris [a], Benedikt Demmert [a], Dorrit E. Jacob [c], Mihail Mondeshki [d], Encarnación Ruiz-Agudo [e], Carlos Rodríguez-Navarro [e]

[a] Department of Materials Science and Engineering, Institute of Glass and Ceramics (WW3), Friedrich-Alexander University Erlangen-Nürnberg (FAU), Martensstrasse 5, 91058 Erlangen, Germany
[b] Interdisciplinary Center for Functional Particle Systems (FPS), Friedrich-Alexander University Erlangen-Nürnberg (FAU), Haberstrasse 9a, 91058 Erlangen, Germany
[c] Department of Earth and Planetary Sciences, 16 University Avenue, Macquarie University, NSW 2109, Australia
[d] Institute of Inorganic and Analytical Chemistry, Johannes Gutenberg-University of Mainz, Duesbergweg 10-14, Germany
[e] Department of Mineralogy and Petrology, University of Granada, Spain, Fuentenueva s/n, 18071 Granada, Spain

ARTICLE INFO

Article history:
Received 31 January 2016
Received in revised form 25 May 2016
Accepted 22 July 2016
Available online 25 July 2016

Keywords:
Biomineralization
Oriented attachment
Amorphous calcium carbonate
ACC
Nanoglobules
PILP
Nonclassical crystallization

ABSTRACT

A distinct nanogranular fine structure is shared by a wealth of biominerals from several species, classes and taxa. This nanoscopic organization affects the properties and behavior of the biogenic ceramic material and confers on them attributes that are essential to their function. We present a set of structure-relationship properties that are rooted in the nanogranular organization and we propose that they rest on a common pathway of formation, a colloid-driven and hence nonclassical mode of crystallization. With this common *modus operandi*, we reveal the most fundamental and wide spread process-structure-property relationship in biominerals. With the recent increase in our understanding of nonclassical crystallization *in vitro* and *in vivo*, this significant process-structure-property relationship will serve as a source for new design approaches of bio-inspired materials.

Introduction

Biominerals serve as an invaluable source of inspiration for materials design and synthesis as their task-optimized properties are derived from complex hierarchical organization from the nano- to the macroscale. Understanding the underlying mechanisms of self-organization and crystallization that control the formation of these bioinorganic materials is a challenging interdisciplinary task which impacts on various fields of research. In medical and clinical research, the effects of degradation and aging on the composite material bone, the development of load-bearing, resorbable bone replacement ceramics (Dorozhkin and Epple, 2002a,b; Hench and Thompson, 2010; Hench, 1991), and pathological mineralization (e.g. nephrolithiasis; see Coe et al., 2016, 2005, 1992) are related topics of major importance. From a geo- or climate science point of view, calcifying species play a major role in determining past environmental conditions. Their fossils act as (paleo-)climate archives on which many climate evolution and climate change studies rely (Cobb et al., 2003; Elderfield and Ganssen, 2000). Discovering fundamental and shared concepts of formation and material design would give new inspiration for all of these fields, provide new impulses for biomimesis and would advance our understanding of biomineralization.

A reductionistic approach—a search for common features across species, taxa and phyla—would aim for the identification of structure-property relationships shared by a large set of biomineralizing organisms. At first sight, this route is barred by the great structural variety of biominerals and their diversified metabolic pathways. Mollusc shells alone feature numerous different hierarchical organizations which are taken from a set of different microstructures (Bøggild, 1930; Taylor, 1964; Taylor et al., 1969), each of which can exhibit subtle deviations depending on its taxonomical species or class (e.g. Böhm et al., 2016). Almost no common structural motif is shared by all, or at least a majority of biominerals, especially if phyla other than the Mollusca are considered (e.g. Brachiopoda). However, the advent of high resolution imaging methods has produced evidence that a remarkable

* Corresponding author at: Department of Materials Science and Engineering, Institute of Glass and Ceramics (WW3), Friedrich-Alexander University Erlangen-Nürnberg (FAU), Martensstrasse 5, 91058 Erlangen, Germany.
E-mail address: stephan.e.wolf@fau.de (S.E. Wolf).

http://dx.doi.org/10.1016/j.jsb.2016.07.016
1047-8477/

number of biominerals, from disparate taxa and phyla, share one uniting structural trait on the nanometer scale: the biominerals in question are composed of space-filling nanosized crystalline building blocks separated by an intergranular organic sheath (see Table 1, or for instance Cuif et al., 2011; Dauphin, 2006; Jacob et al., 2008; Sethmann, 2005; Stolarski et al., 2009; Wolf et al., 2012).

This nanoscale feature is one of the most fundamental levels in the hierarchical organization of biominerals, and therefore contributes – along with all other levels of hierarchy – substantially to the macroscale properties. It is remarkable how certain biominerals are able to unite microscale crystallinity with the mesoscopic structure imposed by the nanogranular building blocks. Several biominerals were de facto shown to behave like a single crystal despite their nanogranular organization; i.e., the spines of several sea urchins species in the Echinometridae family (Oaki and Imai, 2006; Seto et al., 2012), nacre of the pearl oyster *Pinctada fucata* (Oaki and Imai, 2005), the skeleton of the red coral *Corallium rubrum* (Vielzeuf et al., 2010, 2008), calcite spicules of the calcisponge *Pericharax heteroraphis* (Sethmann et al., 2006), and calcite prisms of the bivalve *Pinna nobilis* (Wolf et al., 2012). This material property, i.e. to scatter X-rays like a single crystal and to simultaneously exhibit a nanogranular thus mesoscopic organization, is subsumed under the term mesocrystallinity[1]. Originally coined by Cölfen and Mann (2003a, 2003b), this highly influential material and synthesis concept has received considerable attention ever since, especially in the field of biomimetic crystallization and morphosynthetic crystal design (Cölfen and Antonietti, 2008; De Yoreo et al., 2015; Meldrum and Cölfen, 2008). Mesocrystallinity is not a common trait for all nanogranular biominerals; numerous examples of a low crystallographic order are reported (Cuif et al., 2011) as well as intriguingly complex crystallographic textures such as bending and tilting (Checa et al., 2013a; Olson et al., 2013).

In the first section of this review, we aggregate pertinent reports on the presence of this common nanogranular organic/inorganic composite structure. For the sake of conciseness, we focus on calcifying species as these are the most extensively studied; however, we will also highlight some non-calcareous and pathological examples. This exhaustive register demonstrates for the first time the broad occurrence of this nanoscale feature. In the second section, we assess the impact of this nanogranular fine structure on the macro- to nanoscale properties of the biogenic ceramic. We show that a remarkable number of properties—first and foremost mechanical properties—profit from this nanostructure. In the third part, we link the nanogranular organization with nonclassical, i.e. colloid-driven, crystallization processes *in vivo* and give an overview of recently reported evidence from various species.

It is the objective of this review to raise awareness of this wide spread process-structure-property relationship that affects wide ranging properties of biominerals. We expect that this fundamental relationship will not only help us to better understand the properties of biominerals but will also be an influential source of inspiration for bio-inspired material design. The recent advances in understanding of nonclassical crystallization *in vitro*—summarized in a sequel review by Rodriguez-Navarro et al. (2016)—may pave the way for a successful future mimesis of this fundamental process-structure-property relationship.

[1] The definition of a mesocrystal has undergone some cycles of revision in recent years (Cölfen and Antonietti, 2008, 2005a,b; Faraday Disc., 2012); for the most recent definition, see Bergström et al. (2015). For further information on this concept see also the companion review by Rodriguez-Navarro et al., 2016.

I – Structure: nanogranularity is a wide spread structural trait of biominerals

One of the first reports demonstrating a nanogranular fine structure in biominerals dates back to the 1970s. In 1972, Mutvei reported that "the basic mineral components in the nacreous crystals [in Nautilus] are the aragonitic granules" (Mutvei, 1972) which are depicted in Fig. 1A. Etching revealed that nacre tablets featured a fine structure of vertical stacks of nanosized spheroids about 50–100 nm in diameter (see Fig. 1A). An atomic force microscopy study in 2001 substantiated this claim by evidencing the nanogranular fine structure of columnar nacre in two cephalopod species (Fig. 1B and C; Dauphin, 2001). Note that this fine structure is fully space-filling (see Fig. 1D–F) which is in agreement with recent surface area measurements on biominerals (Yang et al., 2011). In that sense, they are comparable to pure geological or synthetic $CaCO_3$ crystals which do not feature a nanogranular fine structure (Ohnesorge and Binnig, 1993; Orme et al., 2001; Stipp et al., 1994; Stolarski and Mazur, 2005) whereas synthetic mesocrystals are characterized by a high porosity (Wang et al., 2006, 2005; Yang et al., 2011). The observations of Mutvei and Dauphin coincide well with XRD studies which established a typical coherence length of 50–200 nm for calcareous biogenic structures (Aizenberg et al., 1997, 1995; Berman et al., 1993, 1990).

Atomic force microscopy (AFM) in tapping mode provides topographical images along with information about probe-sample interactions in the phase image (Cleveland et al., 1998). The principal source of contrast in phase micrographs arises from material contrast resulting from a change in mechanical properties, adhesion, friction or viscoelasticity (Magonov et al., 1997; McLean and Sauer, 1997). Nearly all phase images reported so far show a cortex of different contrast surrounding each individual granule (e.g. Checa et al., 2013b; Dauphin, 2008, 2001; Rousseau et al., 2005; Wolf et al., 2012), see Fig. 1D–F and Fig. 2E–H, L–P. The nature of the perigranular pellicle is not yet clearly established. The consensus of opinion is that this second phase consists of organic biomolecules comprising the intracrystalline organic matrix (e.g. Baronnet et al., 2008; Bruet et al., 2005; Checa et al., 2013b; Dauphin, 2006, 2001; Li et al., 2006a,b; Nouet et al., 2012; Rousseau et al., 2005; Wolf et al., 2012). However, atomic force microscopy phase images cannot provide conclusive evidence that the cortex is of organic nature. Phase shifts merely indicate variations in the probe-sample interaction potentials. The above-mentioned change of the sample's mechanical properties is one potential source of contrast variation since this change leads to a change in energy dissipation. However, topographical variations can also induce phase shifts. A switch from single probe-surface contact on flat surfaces to a broad interaction contact in grooves or dips is also typically accompanied by a phase contrast. Coincidence of phase contrast with topographical features in the corresponding height image therefore calls for special attention because surface roughness may have caused the phase shift. Simple measures such as applying different sample preparation techniques may eliminate such doubts, e.g. by imaging and comparing polished with freshly cleaved and untreated surfaces. In Fig. 1E a typical phase image obtained from a calcium carbonate biomineral is shown, i.e. the interior of calcitic prisms of the bivalve shell of *Pinna nobilis*. The intergranular contrast is clearly visible but the features notably coincide with topographical variations (Fig. 1D). Fig. 1F depicts a phase image of a freshly cleaved surface of the same specimen. In this second phase mapping, phase variations are also clearly present on top of individual granules, as indicated by white arrows. The different sample preparation method preserved the intergranular (and probably) organic material in positions which do not coincide with topographical features.

Table 1
Overview of species, classes and phyla which feature a nanogranular organization akin to those shown in Figs. 1 and 2. The table claims not to be exhaustive and selects pertinent atomic force microscopy studies.

(Sub)Phylum	Species name	Microstructure	Granule Ø	Comments	Source
Order/(Super)Class	sp. = no subspecies name given			a.a. = accepted as; m.a. = misspelled as	
Brachiopoda					
	Terebratulina retusa	Calcite fibres	600–650 nm		Cusack et al. (2008, 2010)
	Novocrania anomala	Calcite fibres	<100 nm		Perez-Huerta et al. (2013)
	Laqueus rubellus	Calcite fibres	<50 nm		Perez-Huerta et al. (2013)
	Notosaria nigricans	Calcite fibres	<50 nm		Perez-Huerta et al. (2013)
Cnidaria					
Anthoathecata	*Adelopora sp.*		50–100 nm		Stolarski and Mazur (2005)
Anthozoa	*Isastraea sp.*		50–100 nm	Jurassic	Stolarski and Mazur (2005)
	Merulina scabricula		40–100 nm		Cuif and Dauphin (2004)
	Stephanocyathus paliferus		~50 nm		Stolarsky (2003)
Scleractinia	*Caryophyllia smithi*		40–80 nm		Cuif and Dauphin (2004, 2005)
	Cladocora caespitosa		40–80 nm		Cuif and Dauphin (2004, 2005)
	Coelosmilia sp.		30–100 nm	Cretaceous, a.a. Anomocora	Stolarski et al. (2007)
	Desmophyllum sp		30–100 nm		
	Favia stelligera		40–80 nm	a.a. *Goniastrea stelligera*	
			50–100 nm		Stolarski and Mazur (2005)
	Goniastrea retiformis		50–100 nm		Stolarski and Mazur (2005)
	Montastrea sp.		40–80 nm	a.a.: *Montastraea*	Cuif and Dauphin (2005)
	Paracyathus sp.		50–100 nm		Stolarski and Mazur (2005)
	Porites australiensis & lutea		40–80 nm		Cuif and Dauphin (2005)
	Rennensismilia sp.		50–100 nm	Cretaceous	Stolarski and Mazur (2005)
	Trochocyathus sp.		50–100 nm	Cretaceous	Stolarski and Mazur (2005)
Echinodermata					
Echinoidea	*Anthocidaris crassispina*		118 nm ± 44 nm	m.a. *Authoeidaris erassispina*	Seto et al. (2012)
			×43 nm ± 14 nm	a.a. *Heliocidaris crassispina*	
	Balanocrinus berchteni		80–130 nm	Jurassic	Stolarski et al. (2009)
	Chariocrinus andreae		80–130 nm	Jurassic	Stolarski et al. (2009)
Mollusca					
Bivalvia					
	Acila divaricata	Nacre	20–120 nm		Checa et al. (2013b)
	Glycymeris glycymeris	Crossed-lamellar	20–120 nm		Böhm et al. (2016), Wolf et al. (2015)
	Hyriopsis cumingii	Nacre	30–150 nm	Fresh water pearls, cultured	Jacob et al. (2008)
	Mytilus edulis	Fibrous calcite	20–140 nm		Dauphin (2008)
		Nacre	20–140 nm		Dauphin (2008)
	Neotriginia sp.	Unclear	50–75 nm		Dauphin et al. (2014)
	Nucula nitidosa	Nacre	20–120 nm		Checa et al. (2013b)
	Pecten maximus	Foliated calcite	30–100 nm		Dauphin (2008)
	Perna viridis	Nacre	20–120 nm		Checa et al. (2013b)
	Pinctada margaritifera	Calcite prisms	110 x 250–400 nm		Dauphin (2003)
		Calcite prisms	50–75 nm		Cuif et al. (2014)
		Calcite prisms	50–150 nm		Checa et al. (2013a)
		Nacre	20–150 nm		Dauphin (2008), Checa et al. (2013b)
	Pinctada maxima	Nacre	44 ± 23 nm		Rousseau et al. (2005)
		Nacre	38 ± 21 nm		Stempflé and Brendlé (2006)
		Nacre	20–100 nm	Fresh water pearls, cultured	Jacob et al. (2008)
	Pinna nobilis	Calcite prisms	40–140 nm		Dauphin (2008)
		Calcite prisms	20–100 nm	Polished & fractured	Wolf et al. (2012)
		Nacre	20–120 nm		Wolf et al. (2015)
	Pteria hirundo	Nacre	20–120 nm		Checa et al. (2013b)
	Placuna placenta	Calcitic lamellae	30–50 nm		Li and Ortiz (2013)

Table 1 (*continued*)

(Sub)Phylum	Species name	Microstructure	Granule Ø	Comments	Source
Order/(Super)Class	sp. = no subspecies name given			a.a. = accepted as; m.a. = misspelled as	
Gastropoda					
	Bolma rugosa	Nacre	20–120 nm		Checa et al. (2013b)
	Concholepas concholepas	Calcitic prisms	14–140 nm		Dauphin (2003, 2008)
		Crossed-lamellar	15–140 nm		Dauphin (2003, 2008)
	Cypraea sp.	Unclear	30–140 nm		Dauphin (2008)
	Gibbula cineraria	Nacre	20–120 nm		Checa et al. (2013b)
	Gibbula umbilicalis	Nacre	20–120 nm		Checa et al. (2013b)
	Haliotis rufescens	Calcitic prisms	15–100 nm		Dauphin (2008)
		Nacre	20–40 nm		Li et al. (2004) and Li et al. (2006a,b)
			<120 nm		Huang and Li (2012, 2013)
			25–150 nm		Dauphin (2008)
	Haliotis tuberculata	Nacre	30–100 nm		Dauphin (2008)
	Nerita undata	Crossed-lamellar aragonite	50–150 nm		Nouet et al. (2012)
	Trochus niloticus	Nacre	50–75 nm	a.a. *Tectus niloticus*	Bruet et al. (2005)
Cephalopoda					
Nautilida	*Nautilus macromphalus*	Nacre	20–200 nm		Dauphin (2001, 2002, 2006, 2008)
	Nautilus pompilius	Nacre	30–130 nm		Checa et al. (2013)
	Quenstedtoceras sp.	Nacre	<100 nm	Jurassic fossils	Dauphin (2002)
Spirulida	*Spirula spirula*	Nacre	25–120 nm		Dauphin (2001)
Porifera					
Calcarea	*Leuconia johnstoni*	Calcite spicules	60–130 nm		Kopp et al. (2011)
	Pericharax heteroraphis	Calcite spicules	10–30 nm/20–150 nm		Sethmann et al. (2006)
	Petrobiona massiliana	Calcite spicules	50–100 nm		Gilis et al. (2011)
	Petrobiona sp.	Calcite fibres	50–100 nm		Stolarski and Mazur (2005)
Hexactinellida	*Euplectella sp.*	Fibres	30–100 nm	Siliceous	Aizenberg et al. (2005)
Vertrebrata					
Pisces	*Gadus morhua*	Otoliths	<50 nm		Dauphin and Dufour (2008)
Mammalia	*Homo sapiens*	Bone	~50 nm		e.g. Tai et al. (2006), Fantner et al. (2005)
		Kidney stones	<150 nm		Sandersius and Rez (2007)

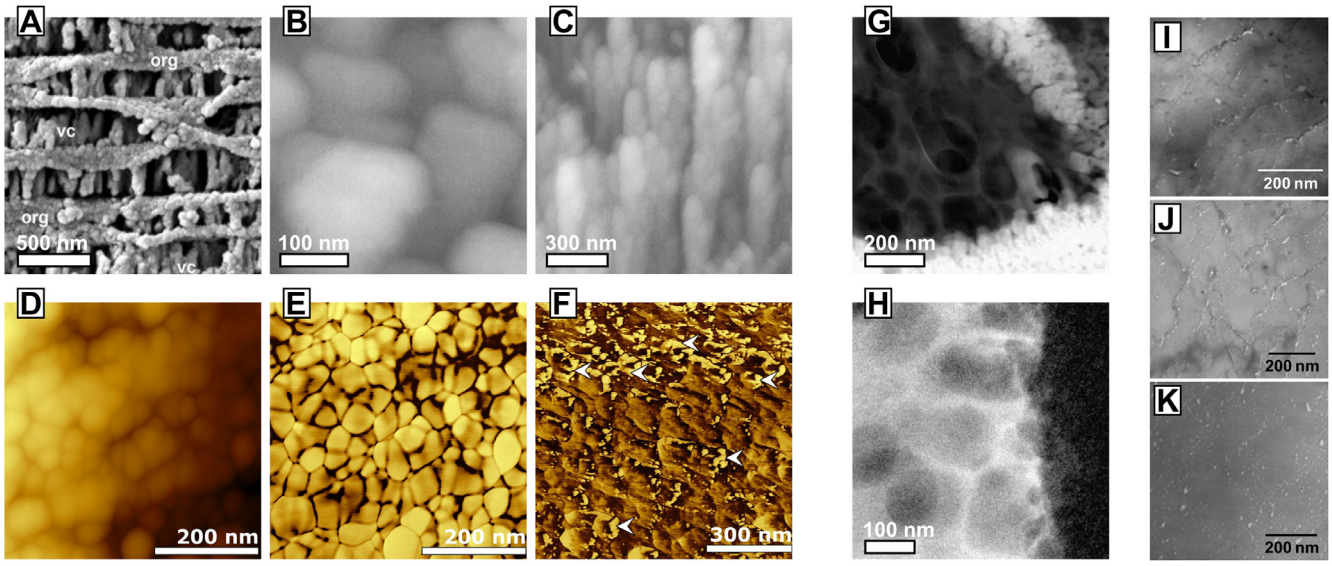

Fig. 1. Evidence for a nanogranular fine structure in molluscan biominerals. **(A)** Etched nacre reveals, besides the organic interlamellar matrix (*org*), vermiculations (*vc*) which are columnar stacks of 50–100 nm mineral granules [Taken from Mutvei and Dunca (2010), with permission of Springer]. **(B, C)** Atomic force micrographs evidence the granular building blocks and rod-like organization of the granules [Taken from Dauphin (2001), with permission of Springer]. **(D–F)** Exemplary height (D) and phase images (E,F) of a nanogranular biomineral – here calcite prisms of *Pinna nobilis*. In (D) and (E) a mirror-polish was applied, in (F) a freshly fractured surface was imaged. Reproduced from Wolf et al. (2012) with permission from The Royal Society of Chemistry]. **(G)** TEM of an area low in electron density adjacent to a granular mineral aggregate in a pearl; **(H)** Electron energy loss element map for carbon of a region in (G) [Reprinted from Jacob et al. (2008) with permission from Elsevier]. **(I–K)** Underfocused bright-field TEM images w of the prisms in *P. fucata* (I), *C. nippona* (J), and *A. pectinata* (K) [Reprinted with permission from Okumura et al., 2012 Copyright 2012 American Chemical Society].

The observation of such contrast variations in regions of single probe-surface contact abates the doubts that the intergranular phase variation is a mere AFM artifact caused by surface roughness (Wolf et al., 2012).

Orthogonal measurement techniques that rest on a different physical phenomenon for signal generation substantiate the assumption of an intergranular organic matrix. Solid-state nuclear magnetic resonance (SS-NMR) suggests the existence of buried inorganic-organic interfaces in biominerals (Ben Shir et al., 2013; Wolf et al., 2015). Transmission electron microscopy (TEM) investigations of pearls substantiated the organic-inorganic nanocomposite structure by revealing a spongy, porous carbon-rich network permeating the biomineral growth layers whose meshes are filled with electron-dense calcium carbonate (see Fig 1G and H; Jacob et al., 2008). Additional TEM studies on four different bivalve species showed a granular organization and the presence of a halo of distinctly lower electron density surrounding the individual nanogranules (Checa et al., 2013a; Okumura et al., 2012). The locus of this electron-sparse moiety coincides with the observations made using tapping-mode AFM, see Fig. 1I to K. Jointly, these studies strongly support the idea that the intergranular matrix is of organic nature. However, conclusive evidence is yet to be provided.

In the case of Mollusca, it was probably Dauphin who first pointed out that their calcified tissues share a "nanostructural unity" (Dauphin, 2008). Nanogranular fine structures were first found by AFM in the class of cephalopods (Checa et al., 2013b; Dauphin, 2008, 2006, 2002, 2001; Mutvei and Dunca, 2010), and were then subsequently identified in the main microstructures of Bivalvia and Gastropoda (see Fig. 2A–C): in sheet nacre (see Fig. 2A; Checa et al., 2013b; Dauphin, 2008; Jacob et al., 2008; Rousseau et al., 2005; Stempflé and Brendlé, 2006; Wolf et al., 2015), prismatic calcite (see Fig. 2B; Checa et al., 2013a; Cuif et al., 2014; Dauphin, 2008, 2003a; Wolf et al., 2015, 2012), foliated calcite (Dauphin, 2008) and in the crossed-lamellar aragonite of bivalves (see Fig. 2C; Böhm et al., 2016; Wolf et al., 2015) as well as in columnar nacre (Bruet et al., 2005; Checa et al., 2013b; Huang and Li, 2013, 2012; Kim et al., 2002; Li et al., 2006a,b) and the crossed-lamellar aragonite of gastropods (Dauphin, 2008, 2003b; Nouet et al., 2012). The constant occurrence of nanogranularity in each of these microstructures is remarkable because a distinct secretion pattern with varying organic composition governs the formation of each respective microstructure (Joubert et al., 2010; Marie et al., 2012; Marin et al., 2014, 2013; Montagnani et al., 2011). Nevertheless, we find a nanogranular organization in all of these microstructures, be they made of calcite or aragonite. This clearly suggests that the mechanisms, which give rise to the nanogranular features, are of a fundamental nature and are not affected by variations in the secretion patterns or the host microstructures.

In addition to the phylum Mollusca, identical nanostructures were identified by AFM in the phylum of calcifying Cnidaria (Cuif and Dauphin, 2005, 2004; Cuif et al., 2004; Stolarski and Mazur, 2005; Stolarski, 2003) and also in the spines and tests of sea urchins (phylum Echinodermata; Seto et al., 2012; Stolarski et al., 2009). The spicular skeletons of calcisponges (phylum Porifera) also consist of nanogranules with cortices (see Fig. 2D; Gilis et al., 2011; Kopp et al., 2011; Sethmann et al., 2006) as do the shells from the phylum Brachiopoda (Cusack et al., 2010, 2008; Perez-Huerta et al., 2013). Nanogranules have also been observed in avian eggshells (Rodríguez-Navarro et al., 2015).

The nanogranular organization of all of these taxonomically diverse calcareous biominerals is surprisingly consistent (see Fig. 2; Table 1 lists contributions in which biominerals were characterized by means of AFM). The granules of most species are of approximately similar diameter[2] ca. 50–120 nm and are (partially) encapsulated by an organic cortex. Only *Terebratulina retusa*, a rhynchonelliform brachiopod, exhibits a distinctly larger granule diameter compared to all other species in other phyla (e.g. the phylum

[2] For estimation of the granule diameter, the method of sample preparation and the apparently non-spherical shape of the granules must be taken into account. In sections and polished samples, for instance, the median diameter of the fraction of the largest granules appears to be a good measure for estimating the granule diameter.

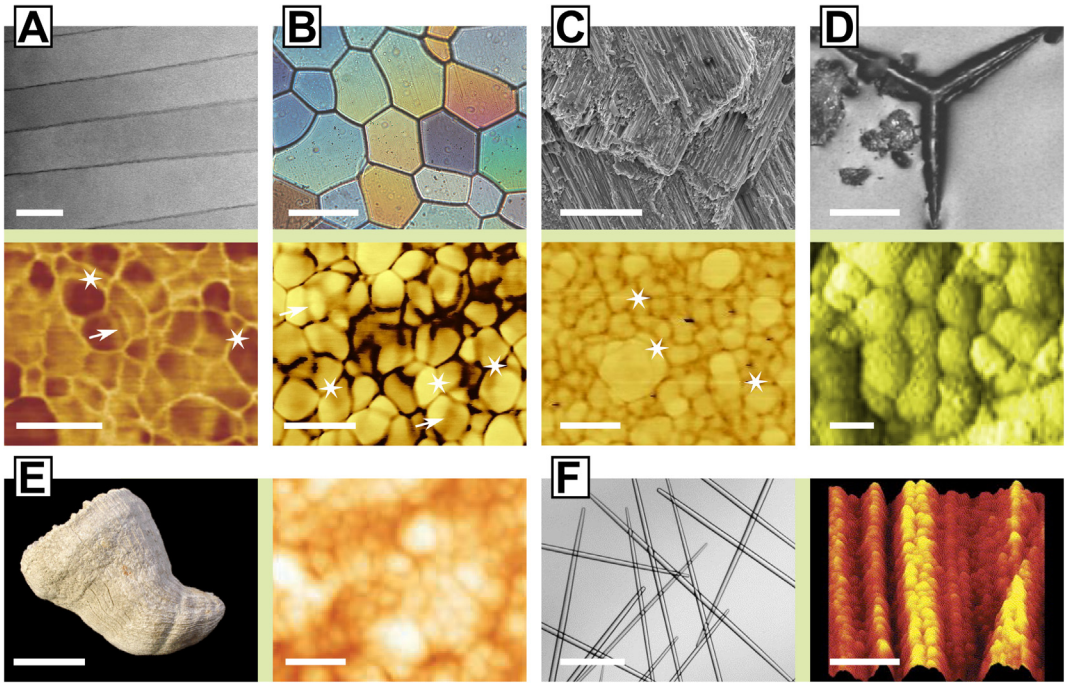

Fig. 2. Atomic force micrographs reveal a common nanogranular organization in various biominerals. **(A-C)** Bivalve microstructures, be they consisted of aragonite (e.g. nacre of *P. maxima* in A, crossed-lamellar aragonite of *G. glycymeris* in C) or calcite (e.g. prisms of *P. nobilis* in B), feature the same granular organization on the nanoscale in tapping-mode atomic force microscopy. Each granule is coated by a perigranular cortex, as shown in the respective phase images. The asterisks exemplify the locus of the intergranular matrix, the so-called cortex. Arrows denote intragranular phase variations within granules that may indicate the existence of intragranular organics. **(D-F)** This nanoscale organization is not restricted to mollusks. Granular nanostructures can be found by AFM topography micrography as fundamental building block in calcisponges (D, *P. heteroraphis*) and silica sponges (E, *T. aurantia*). The nanogranularity can even be preserved in fossils, such as in calcitic Cretaceous coral (F, *Coelosmilia* sp). Scale bars: (A) STEM image: 500 nm, AFM phase image: 100 nm [The latter is reprinted from Rousseau et al. (2005), with permission from Elsevier]; (B) polarized light microscopy image: 40 μm, AFM phase image: 100 nm [The latter is reprinted from Wolf et al. (2012) with permission from The Royal Society of Chemistry]; (C) SEM image: 20 μm, AFM phase image: 100 nm [The latter is reprinted from Böhm et al. (2016) with permission from Cambridge University Press]; (D) Light microscopy image: 100 μm, AFM topography image 100 nm [Reprinted from Sethmann et al. (2006), with permission from Elsevier]; (E) Light microscopy image: 100 μm, AFM topography reconstruction with 2 μm scan size [Reprinted from Weaver et al. (2003), with permission from Elsevier]; (F) Macroscopic image: 20 mm, AFM topography image: 100 nm [Reprinted from Stolarski et al. (2007), with permission from AAAS].

Mollusca) and to other species within the brachiopods (Cusack et al., 2010, 2008; Perez-Huerta et al., 2013). Some species were reported to exhibit a distinctly smaller grain size (<50 nm; see Table 1 or Barthelat et al., 2006; Li et al., 2004; Mutvei and Dunca, 2008; Rousseau et al., 2005; Stempflé and Brendlé, 2006) which may enhance their mechanical properties (see section II on properties). For some species, intragranular phase variations were identified (see white arrows in Fig 1A and B; Dauphin, 2008) which may point to an additional internal grain structure or a fusion of smaller granules into larger ones. Notably, the calcification machinery and secretion profiles of these organisms differ significantly, which is in stark contrast to the observed overarching structural unity of the various phyla. This again points to a fundamental and probably process-related commonality.

Nanogranularity is not restricted to calcareous biominerals, cf. Table 1. The hexactinellid genus *Euplectella* and other demosponges, such as *Thethya aurantia*, are similarly constructed from densely fused nanogranules of silica coated by organics (see Fig. 1E; Sundar et al., 2003; Weaver et al., 2007, 2003). Moreover, we find a similar nanogranular fine structure in bone, i.e. in a biomineral made from highly carbonated hydroxyapatite (Fantner et al., 2005). Also enamel, the hardest biomineral in the human body, consists of 50 nm-sized grains covered with a thin cuticle of organics (Habelitz et al., 2001). Even pathological biomineralization can result in granular features, as seen in kidney stones (Dorian et al., 1996; Lyons Ryall et al., 2001; Sandersius and Rez, 2007a,b; Wolf et al., 2016).

Nanogranularity has even been preserved in fossils (see Fig. 1F); sea urchins from the Jurassic (Stolarski et al., 2009), Createceous corals (Stolarski et al., 2007) and Callovian ammonites (Dauphin, 2002) have been found to feature nanogranularity. This demonstrates the remarkable stability of the nanogranular features.

It has to be stressed that nanogranularity is not a universal trait of all biominerals. Despite the impressive number of biominerals featuring this structural property, there are several examples that exhibit, for instance, well facetted crystals with no distinct fine structure on the nanoscale (Gal et al., 2015). Guanine crystals in fish skins and spider integuments are well studied examples; coccoliths also do not feature any granules on the nanoscale, e.g. *Coccolithus pelagilus* (Henriksen et al., 2004, 2003). We thus advise against using nanogranularity as an unfailing proxy for biogenically formed minerals and against seeing its provenance as a purely vital effect. Moreover, nanogranular features have been frequently observed in minerals formed abiotically; for instance in geological depositions of abiotically precipitated sparry calcite crystals (Stolarski and Mazur, 2005) or *in vitro* precipitation in organic-rich environments (e.g. Kirkland et al., 1999; Sethmann, 2005; see also the sequel to this review). Instead of being of vital provenance, a nanogranular fine structure often indicates nonclassical and colloid-driven mineralization. We know from numerous *in vitro* studies that organic additives, e.g. acidic biomacromolecules (Marin et al., 2013), can act as process-directing agents inducing nonclassical crystallization (Cölfen and Antonietti, 2008). The colloids that drive nonclassical crystallization and accrete to the growing mineral, give rise to a nano- or mesoscopic internal structure. This is especially well-established for a relatively simple but potent *in vitro* biomimetic crystallization model, the so-called polymer-induced liquid-precursor process (PILP, see sequel to this

review, or Gower and Odom, 2000; Gower and Tirrell, 1998; Gower, 2008; Harris et al., 2015; Wolf and Gower, 2016; Wolf et al., 2011a,b, 2008).

II – Properties: nanogranularity affects various properties of biominerals

In the first section of the review we demonstrated that nanogranularity is a common structural feature in biological mineralized tissues; a structural unity of disparate species. In the following part we aim to give an overview of the properties that are affected by this fundamental nanocomposite organization; a compilation of structure-property relationships. Nevertheless, one should always be aware that biominerals are highly hierarchically organized materials. All macroscale properties of biominerals emerge from contributions of each hierarchical level to the respective property. The macroscopic behavior may therefore differ from species to species in accordance with changes in the overall hierarchical organization. For the sake of clarity and rigor of this section, we omit to list other contributing factors and refer to pertinent reviews on a holistic, "materiomic" understanding of hierarchically ordered biogenic and biomimetic materials (Cranford and Buehler, 2012; Cranford et al., 2013; Wegst et al., 2014; etc.).

Dissolution is typically a severe threat to biominerals. The subdivision of a mineral body into nanograins provides several options to tune the solubility of the nanogranular material. Generally speaking, solubility and dissolution is a particle-size-dependent phenomenon. Classical nucleation theory neglects this effect; a simplification known as the capillary assumption (see Dillmann and Meier, 1991, 1989; Ford et al., 1993; as well as the sequel to this review by Rodriguez-Navarro et al., 2016). If the length scale of a nanostructured mineral lies within the capillary regime (i.e., <100 nm), then a distinct deviation from the ideal dissolution behavior has to be expected due to the Gibbs-Thomson effect (typically an increase in solubility; De Yoreo and Vekilov, 2003; Helmholtz, 1886; Perez, 2005; Tolman, 1949, 1948). For the case of enamel—which also features a nanogranular structure—, Tang et al. (2004) demonstrated that this nanoscale organization bestows the biomineral with an inherent resistance to dissolution, probably due to the intergranular matrices. Changing the composition of the intergranular phase can also regulate the dissolution behavior of a biomineral. In the case of rodent teeth enamel, Gordon et al. (2015) showed that the intergranular phase in unpigmented enamel is composed of Mg-substituted amorphous calcium phosphate, whereas the pigmented enamel consists of ferrihydrite and amorphous iron-substituted calcium phosphate. Due to this compositional change, the pigmented layer of rodents is less susceptible to leaching at low pH values.

Due to small particle sizes, it is not only the solubility of mineral phases that can be affected. Such confinement also changes the stability of phases and may thereby change the order of phases in the Ostwald step rule. This phenomenon is well documented for *in vitro* systems (Cantaert et al., 2013; Loste et al., 2004; Stephens et al., 2010; Wang et al., 2013) and also holds true for amorphous calcium carbonate (ACC). Stabilized with a layer of poly(aspartic acid) after synthesis, an intrinsic stability against redissolution was estimated for ACC particles below 100 nm (Nudelman et al., 2010).[3] *In vivo*, we can observe that this phenomenon leads to intracrystalline preservation of amorphous calcium carbonate. Meanwhile, mature calcareous biominerals were repeatedly reported to feature a distinct amount of amorphous calcium carbonate (ACC) embedded within the crystalline mineral body. For instance, XAS on the Ca-K edge revealed 6.9 atom% intracrystalline amorphous calcium carbonate in the mature calcitic prisms of a 25-year-old *Pinna nobilis*. The amorphous fraction in mature *Pinna* prisms is a clear remnant of their genesis via a transient amorphous intermediate (Wolf et al., 2012), a pathway which is established as a generic mechanism for sea urchins as well as for a wide range of other biominerals (Addadi et al., 2006, 2003; Gower, 2008). However, the presence of amorphous materials was expected only for the juvenile development stage until Jacob et al. presented the first direct evidence for ACC in aragonitic mature mollusk shells (Jacob et al., 2011). The preservation of intracrystalline amorphous calcium carbonate was also detected in other aragonitic bivalve microstructures, such as nacre and crossed-lamellar aragonite (Wolf et al., 2015). We extended our SS-NMR study to a set of bivalves with different microstructures: we found about 3 atom% of ACC in *Glycymeris glycymeris* (crossed-lamellar), 3–4% in the calcite prisms of *Pinna nobilis*, and 3–7% intracrystalline ACC in *Tridacna derasa* (crossed-lamellar aragonite, depending on locality within the shell), about 6% in *Arctica islandica* (homogeneous), and up to 10% in *Hyriopsis cumingii* (nacre). It is not clear why in the latter case such a high value is found, but we could verify the presence of ACC by both Raman and TEM (Jacob et al., 2011). We can safely state that all of these bivalves show a distinct intracrystalline fraction of amorphous calcium carbonate substantiating that this preservation is a shared trait of calcareous biominerals. Accordingly, intracrystalline conservation of amorphous calcium carbonate was also reported for other calcareous species, such as sea urchins. Seto et al. (2012) found 5–8 atom% of ACC in mature spines of *Heliocidaris crassispina* and speculated that the intracrystalline amorphous fraction resides at intergranular boundaries and that its transformation is poisoned by the presence of organic material, a proposal similar to the model of Nassif et al. (2005). An additional preservation mechanism was recently proposed by Wolf et al. (2015) which provides an explanation for the relatively large fractions of intracrystalline ACC for which a mere intergranular preservation mechanism cannot account (Wolf et al., 2015). This model was triggered by XANES-PEEM analyses of sea urchin embryo spicules in which mapping of mineral phase distributions revealed small isolated amorphous domains with an approximate diameter of 60–120 nm embedded in a "blue sea" of crystalline materials (see Fig. 3A; Gong et al., 2012). Similar results were recently reported from the growth front of forming nacre (see Fig. 3B; DeVol et al., 2015) and the diameter of these amorphous patches corresponds well with the granule diameter estimated by AFM (see Table 1) or TEM (Checa et al., 2013a; Hovden et al., 2015; Jacob et al., 2008; Okumura et al., 2012; Suzuki et al., 2011). Notably, the same motif, an ACC particle of about 100 nm diameter surrounded by an organic pellicle, was shown to stabilize the amorphous state of the synthetic ACC particle (Nudelman et al., 2010); hence, a similar action of insular grains in a granular nanocomposite is reasonable. Both, the formation pathway via amorphous precursors and the transformation into the stable phase may influence the elemental composition of the end-product. This may carry significant consequences for quantitative paleoclimate reconstruction as noted by Cheng et al. (2007) with respect to the Mg/Ca ratio in biominerals.

The nanogranular organization of a biomineral has a distinct impact on its mechanical behavior. It is as important in biominerals as the microstructure and grain boundaries, which dictate many of the macroscale properties, are in man-made ceramics. Flaws are inherent for brittle ionic crystals, e.g. single grains in (bio)ceramics, and inhibit them from reaching their theoretical maximal strength because defects can act as crack nucleators (Griffith, 1921; Margolin, 1984). Griffith stated that there is a critical length scale below which the fracture strength approaches that

[3] Strictly speaking, the Gibbs-Thomson effect considers the effect of curvature on the solubility of the respective material. A critical radius can only be defined for a perfect sphere. Since the nanogranules are irregular in shape and often oblate, the average granule diameter can only be a rough estimate for assessing if the granules are in the capillary regime.

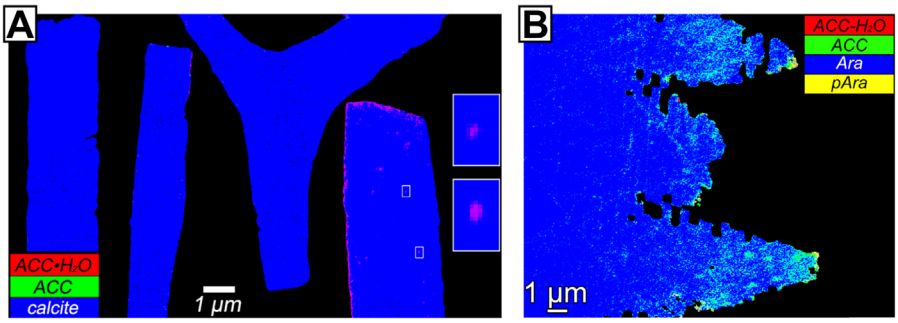

Fig. 3. Mapping experiments reveal anisotropic phase compositions on the nanoscale in early stages of mollusc biomineralization. **(A)** XANES-PEEM documents intracrystalline amorphicity in 72 h old spines of a sea urchin; the insets on the right represent enlarged maps with a pixel size of 20 nm of the boxed region. The magenta nanoparticles are 60–120 nm in size [Taken with permission from Gong et al., 2012]. **(B)** The growth front in nacre of bivalves is also initially amorphous [Reprinted with permission from DeVol et al. (2015) Copyright 2015 American Chemical Society].

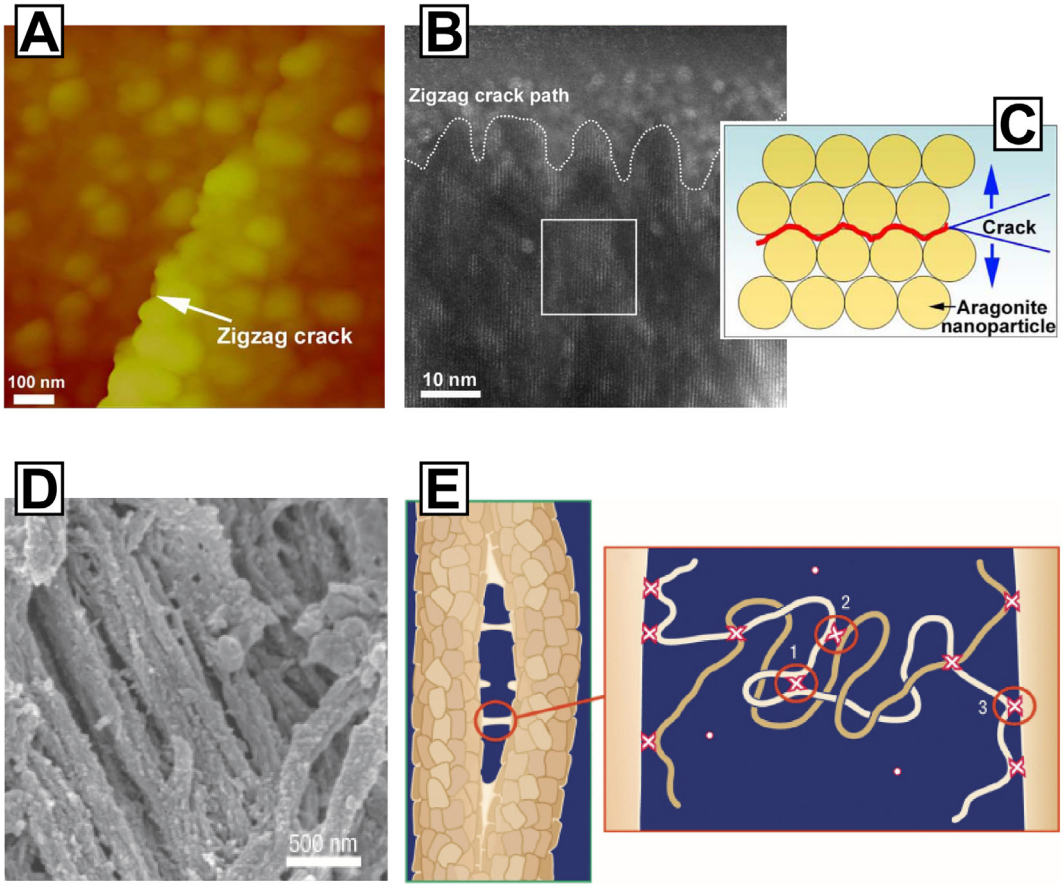

Fig. 4. Crack pathway and ligation in nanogranular bioceramics. **(A–C)** The perigranular crack propagation in nacre significantly enlarges the crack pathway [Reprinted with permission from Macmillan Publishers Ltd: Scientific Reports, Huang and Li (2013), copyright 2013]. **(D)** Crack ligation by the intergranular organic matrix in bone. **(E)** Scheme illustrating sacrificial bonds in the ligating organic matrix; the cation-mediated crosslinks can connect (1) intramolecularly, (2) intermolecularly or (3) generating additional anchoring on the mineral grains. [Reprinted with permission from Macmillan Publishers Ltd: Nature Materials, Fantner et al. (2005), copyright 2005].

of a perfect crystal (Griffith, 1921; Margolin, 1984). By rigorously applying this so-called Griffith criterion, Fratzl and co-workers explained that composites with structures on the nano- to mesoscale may experience optimized strength and a maximum flaw tolerance. Interpreting the intracrystalline organic matrix as intrinsic nanosized cracks in biominerals, they predicted, based on the Griffith criterion, that if a flaw-containing building block is larger than a critical value of about 30 nm, then the mineral building block will fail by stress concentration at the crack tips. However, if the size of the building block drops below this critical length scale, then the intrinsic crack does not accumulate stress at its tips and the building block will not fail by cracking and will resist crack propagation (Gao et al., 2003). Although the characteristic lengths of biomineral microstructures to which Gao et al. referred to are above this threshold (e.g. nacre tablets are several hundred nanometers in thickness), we clearly point out that the typical diameter of nanogranules are near this critical value. Several species were reported to feature a grain size that exactly meets this criterion (see Table 1), e.g. various sea urchins (Oaki and Imai, 2006; Seto et al., 2012), brachiopods (Perez-Huerta et al., 2013) or in nacre of *Pinctada spp.* (Li et al., 2006a,b; Rousseau et al., 2005; Stempflé and Brendlé, 2006; Takahashi et al., 2004).

However, the critical length given above should be seen only as a rough approximation since the derivation does not take into account that the intergranular organic matrix affects crack resistance considerably, as we will see in the following.

As a direct consequence of the considerations above, nanogranularity affects the cracking behavior on the mesoscale and causes the characteristic conchoidal fracture behavior of various biominerals. In single-crystalline aragonite or calcite, a crack follows the characteristic cleavage planes, e.g. along {104} in calcite, which generates the well-known smooth crack surfaces. In a nanogranular material with grain diameters below the critical Griffith value, conchoidal fracture behavior is observed. The individual granules remain intact since they (nearly) reach their theoretical strength and, thus, the crack path is no longer straight and dominated by the crystal cleavage planes. Instead, it runs in tortuous trails through the intergranular organic matrix (the case of nacre is exemplarily shown in Fig. 4A–C). The path length considerably increases; consequently crack travel through the biomineral absorbs more energy (Huang and Li, 2013). This generates irregular crack surfaces that increase frictional resistance and energy consumption for shearing and sliding, similar to the nanoasperites reported for nacre (Barthelat et al., 2006; Evans et al., 2001; Wang et al., 2001).

The perigranular path forces the crack to travel through the proteinaceous matrix which can thereby contribute considerably to energy dissipation. The intergranular organic matrix can bridge a crack of several hundred nanometers since it shows good adhesion to the mineral grains (Fantner et al., 2005; Li et al., 2006a,b; Smith et al., 1999; Sumitomo et al., 2008), see for instance the case of bone in Fig. 4D. The stretching of these bridging "glue molecules" leads to rupture of sacrificial bonds, which are often calcium-mediated (Fantner et al., 2005; Smith et al., 1999). These sacrificial bonds are additional inter-/intramolecular bridges and are typically weak and break before the strong bonds of the polymer backbone (see Fig. 4E). The energy needed to break these bonds increases the overall energy required to advance the crack, and thus the toughness of the material is increased. Additionally, rupture of the sacrificial bonds in the intergranular glue molecules allows unfolding of loops releasing hidden length (e.g. Fig. 4E-1) of the bridging polymer thereby preserving the integrity of the ligament. After relaxation, the sacrificial bonds may reform and the ligament may refold/contract again. This self-healing mechanism in bioceramics was demonstrated for bone (Currey, 2001; Fantner et al., 2005; Thompson et al., 2001) and for nacre (Smith et al., 1999; Sumitomo et al., 2008). Taking the case of pigmented rodent enamel, it seems that replacing iron for calcium (or Mg) in the intergranular matrix strengthens these sacrificial bonds as the hardness is increased considerably (Gordon et al., 2015); this design bears remarkable resemblance to iron-mediated sacrificial and self-healing crosslinks in byssal threads of marine mussels (Harrington et al., 2010)

Stretching of the intergranular organic matrix transmits forces to grains to which a ligation is attached and can consequently lead to nanogranule rotation pushing nearby neighbors of the rotating granules away. Li et al. (2006a,b) reported that this rotation leads, on the one hand, to grain deformation by abrasion and shear (and thus to energy dissipation) and, on the other hand, to an increased spacing between the granules (Li et al., 2006a,b). On the basis of this observation, they claimed that nacre expands under tension, i.e. nacre features a negative Poisson's ratio under tensile stress. In other words, nanogranularity can render biominerals auxetic. Similar observations were made recently in the case of the nonnacreous shell of *P. placenta*, in which, upon nanoindentation, viscoplastic stretching of intergranular organic material was observed along with nanograin detachment and nanograin rotation (Li and Ortiz, 2014, 2013).

Due to a similar combination of nanogranule sliding, organic ligament bridging and nanogranule rotation, nanogranular biominerals feature enhanced plasticity and viscoelastic behavior on the nanoscale. This nanoplasticity was claimed for both nacre (Li et al., 2004; Mohanty et al., 2011) and for bone (Tai et al., 2006). This change in behavior is remarkable since plastic deformation, one fundamental mechanism of energy dissipation, occurs in brittle ionic crystals only under compression or shear by dislocation motion or mass transport. Nanogranularity thus grants a new type of plasticity to the material.

The concept of an intergranular yet intracrystalline organic matrix seems to also provide a method to control the density distribution of organic inclusions which, in turn, may affect mechanical properties and crack propagation. Embedded organic molecules lower the elastic modulus of the ceramic host material locally. Distributing the organic inclusions in an anisotropic fashion can generate a gradient of the elastic modulus that will force the crack to deflect to regions with lower elastic modulus (Younis et al., 2012). Younis et al. recently observed that individual nacre tablets of *Perna canaliculus* feature a thin layer towards the

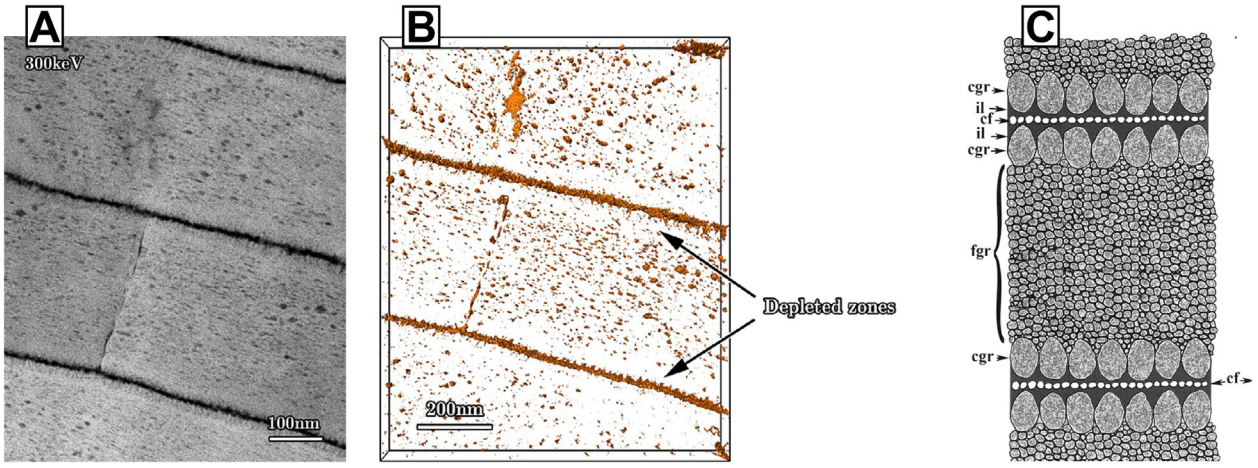

Fig. 5. Nacre tablets featuring zones depleted in intracrystalline organic matrix, evidenced by (**A**) scanning transmission microscopy and (**B**) electron tomography [Adapted with permission from Younis et al. (2012); Copyright 2012 American Chemical Society]. The depletion in organics at the tablet rim can be explained on the basis of Mutvei's observation sketched in subfigure (**C**) that large granules form the outer layer of tablets and that intracrystalline organics mainly reside at the intergranular space [Taken from Mutvei and Dunca (2008), with permission of Springer].

intertabular organic matrix in which the density of intercrystalline organic inclusions is depleted, see Fig. 5 (Younis et al., 2012). They speculated that this inhomogeneous distribution of intracrystalline organic materials may induce the predicted change in cracking behavior. The observation of Younis et al. coincides well with a report by Mutvei and Dunca documenting that the outer layer of nacre tablets in gastropods and cephalopods features a distinctly larger grain size (2008). If the locus of the intracrystalline organic matrix is predominantly at intergranular sites, then variation of grain size may directly control the density of intracrystalline organic inclusions and lead to the anisotropic distribution of the intracrystalline organic matrix and, hence, to areas that are able to deflect cracks.

Last but not least, nanogranules also lead to an increased surface roughness of the building blocks on the next hierarchical level, e.g. nacre tablets, since they serve as their fundamental components. In other words, the nanogranules are the origin of the nanoasperities on the surface of nacre tablets that cause interlocking upon shear and sliding. This considerably increases frictional resistance and energy consumption for shearing and sliding (Barthelat et al., 2006; Evans et al., 2001; Wang et al., 2001).

III – Process: Nonclassical crystallization by colloid attachment and transformation (CAT) as the origin of the nanogranularity of biominerals

In this last section we address the question of from which mechanisms the nanogranularity in biominerals may emanate. Is there a common process from which the set of structure-property relationships listed above may stem? The last decade has brought about an answer to this question as our awareness of nonclassical crystallization processes has increased. A nanogranular fine structure often denotes a colloid-driven and thus nonclassical crystal growth mechanism as has been evidenced in numerous recent studies (Cölfen and Antonietti, 2008; De Yoreo et al., 2015; Gal et al., 2014; Gower, 2008; Meldrum and Cölfen, 2008; see also the companion review by Rodriguez-Navarro et al., 2016). The generation of a granular nanostructure is well established for a distinct mineralization process *via* colloid attachment and transformation (CAT), the so-called polymer-induced liquid-precursor (PILP) process (Gower and Odom, 2000; Gower, 2008; Wolf and Gower, 2016). In this relatively simple but potent biomimetic crystallization model, polyelectrolyte additives such as poly(acrylic acid) or poly(aspartic acid) are used that mimic the charged biopolymers involved in biomineralization *in vivo* (Marin and Luquet, 2007; Marin et al., 2013). During crystallization, they act as process directing agents and shift the crystallization mode from classical to nonclassical growth driven by attachment of amorphous colloids. This CAT process generates nanocomposite materials with nanogranular features indistinguishable from those found in biogenic minerals (Kim et al., 2007; Wolf et al., 2012) and is also capable of creating complex crystallographic textures such as bending and tilting (Harris et al., 2015) similar to those recently identified in mollusk shells (Checa et al., 2013a; Olson et al., 2013).

This suggests that the nanogranular fine structure in biominerals is most likely rooted in a colloid-mediated, nonclassical mode of growth. This idea pairs perfectly with observations of mineral-bearing vesicles in epithelial cells, e.g. ACC-containing vesicles (dubbed "calcosomes" or, more generally, "lithosomes" by Wolf et al., 2012) in calcifying corals (Isa, 1986), sea urchins (Beniash et al., 1999), ciliates (Lemloh, 2015) and bivalves (Neff, 1972; Watabe et al., 1976), or ACP-containing vesicles in osteoblasts (Kerschnitzki et al., 2016; Rohde and Mayer, 2007), bone-lining cells (Mahamid et al., 2011) and ameloblasts (Eisenmann et al., 1979; Garant and Nalbandian, 1968; Kallenbach, 1971; Kim et al., 1994; Reith, 1967). Vesicles bearing a silica precursor, called silicasomes, were also found in silicifying glass sponges (Müller et al., 2008).

Watabe initially suggested that these mineral deposits are activated for mineralization in bivalves by redissolution (Watabe, 1983) but it now also seems reasonable to assume that mineralizing epithelial cells secrete their deposits of amorphous mineral in these "calcosomes" in a colloidal state. It is still under debate

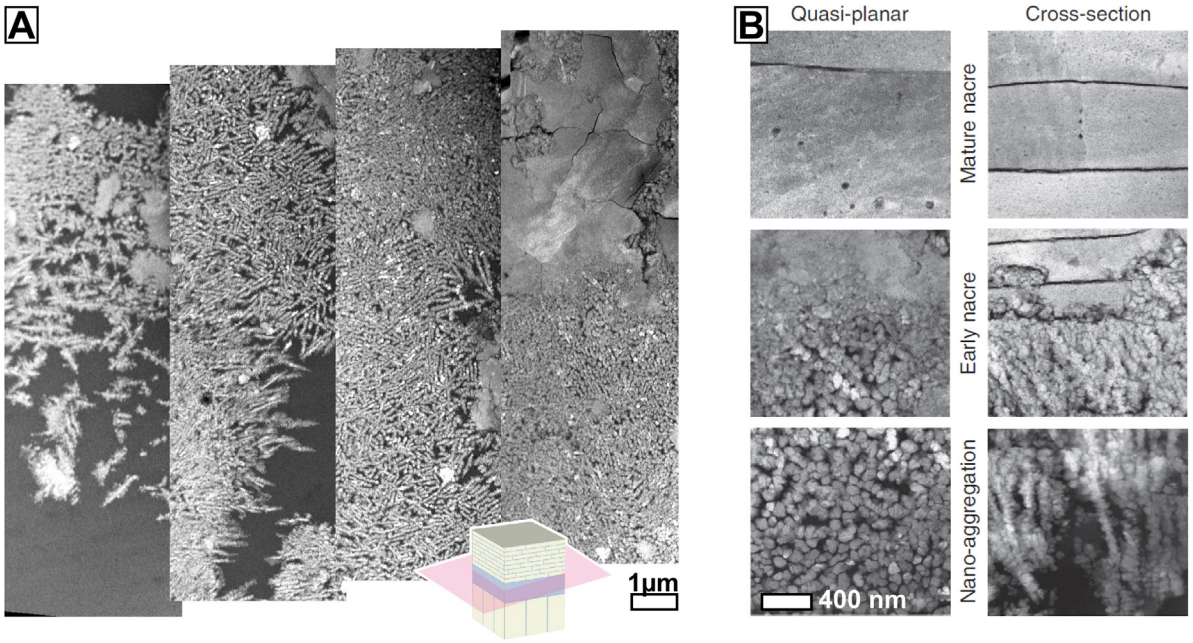

Fig. 6. **(A)** Scanning transmission micrographs of a quasi-planar section through the first layers of nacre in *Pinna nobilis* showing the initial aggregation of colloids which finally turn into fully space-filling nacre. Note the pronounced fibrillar organization preceding tablet formation. **(B)** Detailed views of the different mineralization stages. The stages of early nacre formation reveal how early nacre is formed from the fusion of individual granules [reprinted with permission from Hovden et al., 2015: Copyright Nature Publishing Group].

whether the settling mineral colloid is solid-amorphous and hence particulate (Gal et al., 2015, 2014) or still highly hydrated and hence liquid-condensed (Gower, 2008; Wolf et al., 2012); it may also depend on the mineral the organism precipitates. Nevertheless, the nanostructural unity implies that this colloidal mode of growth is widespread in biomineralization. A colloid-mediated growth process would solve the "logistical problem at the mineralization site" pointed out by Morse and Addadi: for deposition of, for instance, aragonite, "the volume of saturated calcium carbonate solution needed would be at least 10^5 larger than the mineral volume deposited" and would pose high demand "in terms of transporting sufficient mineral to the site and removing large volumes of water" (Addadi et al., 2006).

By means of scanning transmission electron microscopy (STEM) analysis of the onset of nacre in *Pinna nobilis*, i.e. its first layers of nacre, we were able to provide conclusive evidence for a colloid-mediated growth process of bivalve nacre (see Fig. 6; Hovden et al., 2015). Nacre growth starts by aggregation of colloids (Fig. 6, nano-aggregation). As growth progresses, the particle number density increases and, when a critical density is reached, continuous albeit irregular early-nacre layers are formed. High-resolution images of this moment of transformation reveal how the colloids "merge" into space-filling mineral tablets (see Fig. 6, early nacre) this clearly corroborates the assumption of a colloid-mediated growth process in nacre. It is still unclear, what gives rise to the fibrillar organization, be it columnar growth or a templating effect by a fibrillar matrix component such as chitin (Hovden et al., 2015). Despite this unanswered question, the findings bridge nicely with Mutvei's observations of intratabular rod-like vermiculations (see Fig. 1) in nacre and the pertinent nanogranular features observed by AFM (Figs. 1 and 2).

These studies were conducted on nacre of a mature specimen; hence, the initial mineral phase—at the moment of secretion or attachment—could not be determined. However, recent XANES-PEEM mapping showed that the nacre growth interface, which faces the mineralizing epithelial mantle cells, is essentially amorphous in its early stages (see Fig. 3 or DeVol et al., 2015). Similarly, Zhang et al. showed for *Perna viridis* that the initial nacre tablets are only partially crystalline and that they transform into crystalline tablets and, in their semi-crystalline state, are composed of granules not all of which are crystalline (Zhang and Xu, 2013). Similar observations were made by Baronnet et al. (2008) in *Pinctada margaritifera* and by Jacob et al. in cultured pearls of *P. maxima* (Jacob et al., 2008). These observations are all in line with the now established tenet that calcareous (and some other) biominerals form via an amorphous and transient precursor that transforms over the course of time into a crystalline phase (Addadi et al., 2006, 2003; Aizenberg et al., 1996; Beniash et al., 2009; Dillaman et al., 2005; Gago-Duport et al., 2008; Gower, 2008; Hasse et al., 2000; Mahamid et al., 2008; Nassif et al., 2005; Politi et al., 2006; Sethmann et al., 2006; Towe and Lowenstam, 1967; Weiner and Addadi, 2011, 1997; Weiner et al., 2005).

In the following, we outline a schematic model that explains the genesis of nanogranular features in biominerals. The complete process can be paraphrased as a nonclassical crystallization that proceeds via colloid attachment and transformation (CAT) of an amorphous precursor. This precursor is formed and stabilized intracellularly in mineral-bearing "lithosomes". A plausible scenario would be that these lithosomes are exocytosed, be it to an extracellular scaffold or a vesicle-delineated syncytium, attach to and subsequently merge with the growing biomineral in a still amorphous state (Fig. 7A). An alternative setting would be that the lithosomal mineral deposits are first re-dissolved and the resulting ions are secreted to the extracellular mineralizing fluid along with biomacromolecules (Fig. 7B). These polyelectrolytes, akin to the process-directing agents of *in vitro* studies, may lead to an extracellular formation of amorphous mineral-precursor colloids which then, instead of ions, drive the mineralization process in a nonclassical fashion. In both scenarios, the accretion step of the colloids is probably accompanied by dehydration processes

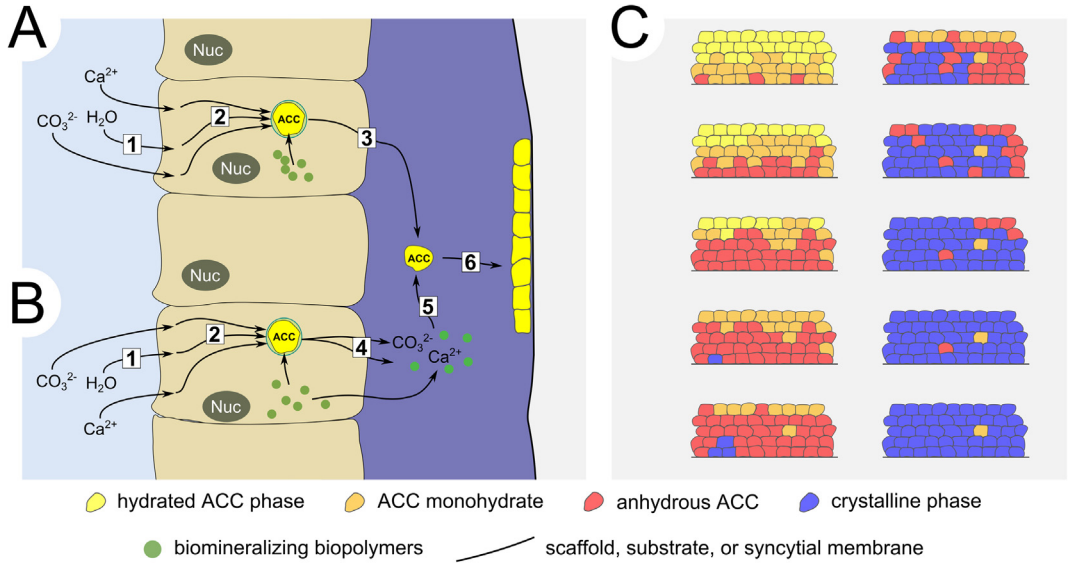

Fig. 7. Possible nonclassical pathways in biotic mineralization that follow a colloid attachment and transformation (CAT) mechanism, here exemplified for the case of a calcium carbonate mineralizing system. **(A, B)** Possible transportation channels that can give rise to nonclassical crystallization. The mineral constituents and water are delivered to the cell (1) which stores them intracellularly in a mineral-bearing vesicle, the litho- or calcosome (2). The amorphous and colloidal content of the calcosome is either exocytosed completely (3) or transported to the mineralization site via re-dissolution (4). In the latter case, concomitantly secreted acidic proteins induce reformation of amorphous precursor colloids (5). The amorphous mineral colloid attaches to the growing mineral interface (6). **(C)** Maturation of the deposited mineral to a fully space-filling mesocrystal. After attachment, the highly hydrated ACC phase (yellow) subsequently loses water (yellow → orange → red) until it is fully dehydrated and ready for crystallization (red → blue). The crystallization can be triggered by heteroepitaxy and the crystallinity percolates through the mineral body by homoepitaxial maturation of the individual nanogranules. Some granules do not transform; either they are shielded by a thick organic cortex or they may be poisoned against crystallization, e.g. due to improper stoichiometry.

(DeVol et al., 2015; Gong et al., 2012; Politi et al., 2008) that lead to the formation of an anhydrous volume of mineral that is ready to undergo a phase transformation from solid-amorphous to solid-crystalline. This phase transformation is pseudomorphic, which means that the resulting mineral morphology deviates from the normal characteristics expressed by a mineral phase formed in equilibrium, and hence preserves the internal nanogranular structure reflecting the fundamental building blocks of the biomineral.

The phase transformation into a crystalline mineral represents the second step in this nonclassical biomineralization process (see Fig. 7C). Primary nucleation of the still amorphous body is probably triggered heteroepitaxially by exploiting the templating action of specific proteinaceous nucleators (Addadi and Weiner, 1985; Belcher et al., 1996; Falini et al., 1996; He et al., 2003; Levi-Kalisman et al., 1998; Nudelman et al., 2007). Once a crystalline granule exists in the amorphous body, maturation of the amorphous monolith advances and percolates through the amorphous mineral body in a random and tortuous path (Politi et al., 2008; Seto et al., 2012; Weiner and Addadi, 2011). Homoepitaxial nucleation induces crystallization of the granules in contact with an already crystallized granule and crystallinity propagates through the mineral volume by "hopping" from granule to granule (Killian et al., 2009; Seto et al., 2012; Weiner and Addadi, 2011; Wolf et al., 2012). Sporadic granules seem to withstand epitaxial nucleation which may be due to their non-stoichiometric composition or a dense and organic cortex impervious enough to preserve individual granules. The process of colloid attachment and transformation (CAT) can give rise to highly crystallographically co-oriented nanogranules, i.e. a mesocrystal, if the propagation of the crystalline phase through the amorphous body is governed by a homoepitaxial templating action of the crystalline bulk phase.

The process of CAT must clearly be delineated from the process of oriented attachment (OA); both of which can lead to the formation of a mesocrystal. In the latter case of OA, *crystalline* mineral particles attach to an already crystalline bulk material in a crystallographic register (Cölfen and Mann, 2003c, 2003d; Li et al., 2012; Penn and Banfield, 1998; Penn and Soltis, 2014; Penn, 1998; see also the companion review by Rodriguez-Navarro et al., 2016) whereas in the case of CAT *amorphous* colloids attach to the growing and not necessarily crystalline mineral body (Addadi et al., 2003; Gower, 2008; Wolf and Gower, 2016). Amorphous materials are intrinsically isotropic and, therefore, cannot undergo oriented attachment (see for instance Homeijer et al., 2010). Sufficient evidence has been provided that the growth of calcareous and apatitic biominerals proceeds via an amorphous precursor (Addadi et al., 2003; Gower, 2008 and references therein; Sviben et al., 2016) and that the crystalline state is achieved by a solid-to-solid phase transformation (Beniash et al., 2009; DeVol et al., 2015; Gong et al., 2012; Wolf et al., 2012). However, biogenic CAT processes have occasionally been, incorrectly described as oriented attachment (e.g. Oaki and Imai, 2006; Zhang and Xu, 2013). Besides the confusion caused by these dichotomous pathways in nonclassical crystallization, we believe that another aspect in this process demands terminological clarification. The templating action of the already crystalline bulk material in CAT processes (Fig. 7C) is often referred to as secondary nucleation, in reference to the chronology of nucleation events. In the field of industrial crystallization, secondary nucleation denotes nucleation processes which occur "*only because* of the presence of crystals of the material which is crystallized" (Botsaris, 1976, italics in original) and is commonly attributed to the generation of secondary nuclei by fluid shear, e.g. by collision of crystals with solid surfaces (e.g. walls of the crystallization unit) or other already existing crystals (McCabe et al., 2004; Tavare, 1995; Evans et al., 1974; Kane et al., 1974). It is obvious that this notion is in conflict with the scenario of a solid-amorphous to solid-crystalline transformation occurring in biominerals. It seems more appropriate to adopt the terminology developed in epitaxy and mineralogy and to refer to the maturation of a biomineral as homo- or isoepitaxy. These terms describe the special case where the substrate is of the same composition as the newly deposited layer and that it templates the formation of the same crystal phase (Herman et al., 2004).

Conclusions & perspectives

Nanogranularity is a common, although not omnipresent feature, of calcareous biominerals and can also be found in other biominerals made from calcium phosphate or silica. This structural characteristic unites microstructures, species, and phyla. It represents an inorganic-organic nanocomposite structure. A wide range of properties rest on this nanocomposite design, namely dissolution resistance, amorphous phase stabilization, self-healing and various mechanical properties, i.e. strength, toughness and fracture behavior. These structure-property relationships emerge from a common colloid-driven mineralization pathway. The nonclassical mineralization pathway lays the basis for one of the most important and most fundamental nanoscale process-structure-property relationship so far identified in biominerals.

Nature demonstrates that, by mastering mineralization by colloid attachment and transformation (CAT), a synthesis pathway to mesocrystalline nanoceramics is opened. Further detailed elucidation of by which means the genesis of crystallographic properties can be controlled, will pave the way to new material synthesis concepts for bio-inspired ceramic materials when paired with advanced understanding of nonclassical processes.

Acknowledgements

SEW is beholden to the German Research Foundation (DFG) for generous financial support in the framework of an Emmy Noether starting grant (N° WO1712/3-1) and further gratefully acknowledges additional financial support by the Bavarian Research Alliance. SEW and JH acknowledge generous financial support from Cluster of Excellence 315 'Engineering of Advanced Materials—Hierarchical Structure Formation for Functional Devices' funded by the German Research Foundation. DEJ is financed by an ARC Future Fellowship at Macquarie University. CRN and ERA thanks for funding by the Spanish Government (Grants MAT2012-37584 and CGL2012-35992) and the Junta de Andalucia (Research Group RNM-179 and Project P11-RNM-7550). E.R.-A. acknowledges a Ramon y Cajal grant.

References

Addadi, L., Weiner, S., 1985. Interactions between acidic proteins and crystals: stereochemical requirements in biomineralization. Proc. Nat. Acad. Sci. USA 82, 4110–4114.

Addadi, L., Raz, S., Weiner, S., 2003. Taking advantage of disorder: amorphous calcium carbonate and its roles in biomineralization. Adv. Mater. 15, 959–970. http://dx.doi.org/10.1002/adma.200300381.

Addadi, L., Joester, D., Nudelman, F., Weiner, S., 2006. Mollusk shell formation: a source of new concepts for understanding biomineralization processes. Chem. Eur. J. 12, 980–987. http://dx.doi.org/10.1002/chem.200500980.

Aizenberg, J., Hanson, J., Koetzle, T.F., Leiserowitz, L., Weiner, S., Addadi, L., 1995. Biologically induced reduction in symmetry: a study of crystal texture of calcitic sponge spicules. Chem. Eur. J. 1, 414–422. http://dx.doi.org/10.1002/ejic.200600428.

Aizenberg, J., Lambert, G., Addadi, L., Weiner, S., 1996. Stabilization of amorphous calcium carbonate by specialized macromolecules in biological and synthetical precipitates. Adv. Mater., 222–226

Aizenberg, J., Hanson, J., Koetzle, T.F., Weiner, S., Addadi, L., 1997. Control of macromolecule distribution within synthetic and biogenic single calcite crystals. J. Am. Chem. Soc. 119, 881–886. http://dx.doi.org/10.1021/ja9628821.

Aizenberg, J., Weaver, J.C., Thanawala, M.S., Sundar, V.C., Morse, D.E., Fratzl, P., 2005. Skeleton of Euplectella sp.: structural hierarchy from the nanoscale to the macroscale. Science 309, 275–278. http://dx.doi.org/10.1126/science.1112255.

Baronnet, A., Cuif, J.-P., Dauphin, Y., Farre, B., Nouet, J., 2008. Crystallization of biogenic Ca-carbonate within organo-mineral micro-domains. Structure of the calcite prisms of the Pelecypod *Pinctada margaritifera* (Mollusca) at the submicron to nanometre ranges. Miner. Mag. 72, 617–626.

Barthelat, F., Li, C.-M., Comi, C., Espinosa, H.D., 2006. Mechanical properties of nacre constituents and their impact on mechanical performance. J. Mater. Res. 21, 1977–1986. http://dx.doi.org/10.1557/jmr.2006.0239.

Belcher, A.M., Wu, X.H., Christensen, R.J., Hansma, P.K., Stucky, G.D., Morse, D.E., 1996. Control of crystal phase switching and orientation by soluble mollusc-shell proteins. Nature. http://dx.doi.org/10.1038/381056a0.

Ben Shir, I., Kababya, S., Katz, I., Pokroy, B., Schmidt, A., 2013. Exposed and buried biomineral interfaces in the aragonitic shell of *Perna canaliculus* revealed by solid-state NMR. Chem. Mater. 25, 4595–4602. http://dx.doi.org/10.1021/cm4028226.

Beniash, E., Addadi, L., Weiner, S., 1999. Cellular control over spicule formation in sea urchin embryos: a structural approach. J. Struct. Biol. 125, 50–62. http://dx.doi.org/10.1006/jsbi.1998.4081.

Beniash, E., Metzler, R.A., Lam, R.S.K., Gilbert, P.U.P.A., 2009. Transient amorphous calcium phosphate in forming enamel. J. Struct. Biol. 166, 133–143. http://dx.doi.org/10.1016/j.jsb.2009.02.001.

Bergström, L., Sturm (née Rosseeva), E.V., Salazar-Alvarez, G., Cölfen, H., 2015. Mesocrystals in biominerals and colloidal arrays. Acc. Chem. Res. 150504141715009. http://dx.doi.org/10.1021/ar500440b.

Berman, A., Addadi, L., Kvick, A., Leiserowitz, L., Nelson, M., Weiner, S., 1990. Intercalation of sea urchin proteins in calcite: study of a crystalline composite material. Science 250, 664–667. http://dx.doi.org/10.1126/science.250.4981.664.

Berman, A., Hanson, J., Leiserowitz, L., Koetzle, T.F., Weiner, S., Addadi, L., 1993. Biological control of crystal texture: a widespread strategy for adapting crystal properties to function. Science 259, 776–779. http://dx.doi.org/10.1126/science.259.5096.776.

Bøggild, O.B., 1930. The Shell Structure of the Mollusks. A.F. Høst & søn, København.

Böhm, C.F., Demmert, B., Harris, J., Fey, T., Marin, F., Wolf, S.E., 2016. Structural commonalities and deviations in the hierarchical organization of crossed-lamellar shells: a case study on the shell of the Bivalve *Glycymeris glycymeris*. J. Mater. Res., accepted

Botsaris, G.D., 1976. Secondary nucleation. In: Mullin, J.W. (Ed.), Industrial Crystallization, pp. 3–22.

Bruet, B.J.F., Qi, H.J., Boyce, M.C., Panas, R., Tai, K., Frick, L., Ortiz, C., 2005. Nanoscale morphology and indentation of individual nacre tablets from the gastropod mollusc trochus niloticus. J. Mater. Res. 20, 2400–2419. http://dx.doi.org/10.1557/jmr.2005.0273.

Cantaert, B., Beniash, E., Meldrum, F.C., 2013. Nanoscale Confinement Controls the Crystallization of Calcium Phosphate: Relevance to Bone Formation. Chem. - A Eur. J. 19, 14918–14924. http://dx.doi.org/10.1002/chem.201302835.

Checa, A.G., Bonarski, J.T., Willinger, M.G., Faryna, M., Berent, K., Kania, B., González-Segura, A., Pina, C.M., Pospiech, J., Morawiec, A., 2013a. Crystallographic orientation inhomogeneity and crystal splitting in biogenic calcite. J. R. Soc. Interf. 10, 20130425. http://dx.doi.org/10.1098/rsif.2013.0425.

Checa, A.G., Mutvei, H., Osuna-Mascaró, A.J., Bonarski, J.T., Faryna, M., Berent, K., Pina, C.M., Rousseau, M., Macías-Sánchez, E., 2013b. Crystallographic control on the substructure of nacre tablets. J. Struct. Biol. 183, 368–376. http://dx.doi.org/10.1016/j.jsb.2013.07.014.

Cheng, X., Varona, P.L., Olszta, M.J., Gower, L.B., 2007. Biomimetic synthesis of calcite films by a polymer-induced liquid-precursor (PILP) process. J. Cryst. Growth 307, 395–404. http://dx.doi.org/10.1016/j.jcrysgro.2007.07.006.

Cleveland, J.P., Anczykowski, B., Schmid, A.E., Elings, V.B., 1998. Energy dissipation in tapping-mode atomic force microscopy. Appl. Phys. Lett. 72, 2613–2615.

Cobb, K.M., Charles, C.D., Cheng, H., Edwards, R.L., 2003. El Niño/Southern Oscillation and tropical Pacific climate during the last millennium. Nature 424, 271–276. http://dx.doi.org/10.1038/nature01779.

Coe, F.L., Evan, A., Worcester, E., 2005. Kidney stone disease. J. Clin. Invest. 115, 2598–2608. http://dx.doi.org/10.1172/JCI26662.

Coe, F.L., Worcester, E.M., Lingeman, J.E., Evan, A.P. (Eds.), 2016. Kidney Stones: Medical and Surgical Management. Jaypee Medical Publishers, Philadelphia, PA.

Cölfen, H., Antonietti, M., 2005a. Mesokristalle: anorganische Überstrukturen durch hochparallele Kristallisation und kontrollierte Ausrichtung. Angew. Chem. 117, 5714–5730. http://dx.doi.org/10.1002/ange.200500496.

Cölfen, H., Antonietti, M., 2005b. Mesocrystals: inorganic superstructures made by highly parallel crystallization and controlled alignment. Angew. Chem. Int. Ed. 44, 5576–5591. http://dx.doi.org/10.1002/anie.200500496.

Cölfen, H., Antonietti, M., 2008. Mesocrystals and Nonclassical Crystallization. Wiley-VCH Verlag GmbH.

Cölfen, H., Mann, S., 2003a. Geordnete mesoskopische Strukturen durch Selbstorganisation und Transformation von Hybrid-Nanostrukturen. Angew. Chem. 115, 2452–2468. http://dx.doi.org/10.1002/ange.200200562.

Cölfen, H., Mann, S., 2003b. Higher-order organization by mesoscale self-assembly and transformation of hybrid nanostructures. Angew. Chem. – Int. Ed. 42, 2350–2365. http://dx.doi.org/10.1002/anie.200200562.

Cölfen, H., Mann, S., 2003c. Higher-order organization by mesoscale self-assembly and transformation of hybrid nanostructures. Angew. Chem. Int. Ed. 42, 2350–2365. http://dx.doi.org/10.1002/anie.200200562.

Cranford, S.W., Buehler, M.J., 2012. Biomateriomics. Springer.

Cranford, S.W., de Boer, J., van Blitterswijk, C., Buehler, M.J., 2013. Materiomics: An -omics Approach to Biomaterials Research. Adv. Mater. 25, 802–824. http://dx.doi.org/10.1002/adma.201202553.

Cuif, J.-P., Dauphin, Y., 2004. The environment recording unit in coral skeletons: structural and chemical evidences of a biochemically driven stepping-growth process in coral fibres. Biogeosciences Discuss. 1, 625–658. http://dx.doi.org/10.5194/bgd-1-625-2004.

Cuif, J.-P., Dauphin, Y., 2005. The two-step mode of growth in the scleractinian coral skeletons from the micrometre to the overall scale. J. Struct. Biol. 150, 319–331. http://dx.doi.org/10.1016/j.jsb.2005.03.004.

Cuif, J.-P., Dauphin, Y., Berthet, P., Jegoudez, J., 2004. Associated water and organic compounds in coral skeletons: quantitative thermogravimetry coupled to infrared absorption spectrometry. Geochem. Geophys. Geosystems 5. http://dx.doi.org/10.1029/2004GC000783.

Cuif, J.-P., Dauphin, Y., Sorauf, J.E., 2011. Biominerals and Fossils Through Time. Cambridge University Press.

Cuif, J.-P., Burghammer, M., Chamard, V., Dauphin, Y., Godard, P., Moullac, G., Nehrke, G., Perez-Huerta, A., 2014. Evidence of a biological control over origin, growth and end of the calcite prisms in the shells of *Pinctada margaritifera* (Pelecypod, Pterioidea). Minerals 4, 815–834. http://dx.doi.org/10.3390/min4040815.

Currey, J., 2001. Sacrificial bonds heal bone. Nature 414, 699. http://dx.doi.org/10.1038/414699a.

Cusack, M., Dauphin, Y., Chung, P., Perez-Huerta, A., Cuif, J.-P., 2008. Multiscale structure of calcite fibres of the shell of the brachiopod *Terebratulina retusa*. J. Struct. Biol. 164, 96–100. http://dx.doi.org/10.1016/j.jsb.2008.06.010.

Cusack, M., Chung, P., Dauphin, Y., Pe, A., 2010. Brachiopod primary layer crystallography and nanostructure. Paleonotology 84, 99–105. http://dx.doi.org/10.1111/j.1475-4983.2010.00977.x.

Dauphin, Y., 2001. Nanostructures de la nacre des tests de céphalopodes actuels; nanostructures of the nacreous layers in recent cephalopod shells. Paläontologische Zeitschrift 75, 113–122.

Dauphin, Y., 2002. Fossil organic matrices of the Callovian aragonitic ammonites from Lukow (Poland): location and composition. Int. J. Earth Sci. 91, 1071–1080. http://dx.doi.org/10.1007/s00531-002-0262-2.

Dauphin, Y., 2003a. Soluble organic matrices of the calcitic prismatic shell layers of two *Pteriomorphid bivalves*. *Pinna nobilis* and *Pinctada margaritifera*. J. Biol. Chem. 278, 15168–15177. http://dx.doi.org/10.1074/jbc.M204375200.

Dauphin, Y., 2003b. Microstructure, nanostructure and composition of the shell of *Concholepas concholepas* (Gastropoda, Muricidae). Aquat. Living Resour. 16, 95–103. http://dx.doi.org/10.1016/S0990-7440(03)00022-6.

Dauphin, Y., 2006. Structure and composition of the septal nacreous layer of *Nautilus macromphalus* L. (Mollusca, Cephalopoda). Zoology 109, 85–95. http://dx.doi.org/10.1016/j.zool.2005.08.005.

Dauphin, Y., 2008. The nanostructural unity of Mollusc shells. Miner. Mag. 72, 243–246. http://dx.doi.org/10.1180/minmag.2008.072.1.243.

Dauphin, Y., Dufour, E., 2008. Nanostructures of the aragonitic otolith of cod (Gadus morhua). Micron 39, 891–896. http://dx.doi.org/10.1016/j.micron.2007.11.007.

Dauphin, Y., Cuif, J., Castillo-Michel, H., Chevallard, C., Farre, B., Meibom, A., 2014. Unusual micrometric calcite-aragonite interface in the abalone shell haliotis (Mollusca, Gastropoda). Microsc. Microanal. 20, 276–284. http://dx.doi.org/10.1017/S1431927613013718.

De Yoreo, J.J., Vekilov, P.G., 2003. Principles of crystal nucleation and growth. Rev. Mineral. Geochem. 54, 57–93. http://dx.doi.org/10.2113/0540057.

De Yoreo, J.J., Gilbert, P.U.P.A., Sommerdijk, N.A.J.M., Penn, R.L., Whitelam, S., Joester, D., Zhang, H., Rimer, J.D., Navrotsky, A., Banfield, J.F., Wallace, A.F., Michel, F.M., Meldrum, F.C., Cölfen, H., Dove, P.M., 2015. Crystallization by particle attachment in synthetic, biogenic, and geologic environments. Science 349. http://dx.doi.org/10.1126/science.aaa6760.

DeVol, R.T., Sun, C.-Y., Marcus, M.A., Coppersmith, S.N., Myneni, S.C.B., Gilbert, P.U.P.A., 2015. Nanoscale transforming mineral phases in fresh nacre. J. Am. Chem. Soc. 151007153715000. http://dx.doi.org/10.1021/jacs.5b07931.

Dillaman, R., Hequembourg, S., Gay, M., 2005. Early pattern of calcification in the dorsal carapace of the blue crab, *Callinectes sapidus*. J. Morphol. 263, 356–374. http://dx.doi.org/10.1002/jmor.10311.

Dillmann, A., Meier, G.E.A., 1989. Homogeneous nucleation of supersaturated vapors. Chem. Phys. Lett. 160, 71–74. http://dx.doi.org/10.1016/0009-2614(89)87558-X.

Dillmann, A., Meier, G.E.A., 1991. A refined droplet approach to the problem of homogeneous nucleation from the vapor phase. J. Chem. Phys. 94, 3872. http://dx.doi.org/10.1063/1.460663.

Faraday Disc., F., 2012. General discussion. Faraday Disc. 136, 103. http://dx.doi.org/10.1039/c2fd90027k.

Dorian, H.H., Rez, P., Drach, G.W., 1996. Evidence for aggregation in oxalate stone formation: atomic force and low voltage scanning electron microscopy. J. Urol. 156, 1833–1837.

Dorozhkin, S.V., Epple, M., 2002a. Biological and medical significance of calcium phosphates. Angew. Chemie Int. Ed. 41, 3130–3146. http://dx.doi.org/10.1002/1521-3773(20020902)41:17.

Dorozhkin, S.V., Epple, M., 2002b. Die biologische und medizinische Bedeutung von Calciumphosphaten. Angew. Chem. 114, 3260–3277. http://dx.doi.org/10.1002/1521-3757(20020902)114:17.

Eisenmann, D.R., Ashrafi, S., Neiman, A., 1979. Calcium transport and the secretory ameloblast. Anat. Rec. 193, 403–422.

Elderfield, H., Ganssen, G., 2000. Past temperature and δ18O of surface ocean waters inferred from foraminiferal Mg/Ca ratios. Nature 405, 442–445. http://dx.doi.org/10.1038/35013033.

Evans, T., Margolis, G., Sarofim, A., 1974. Mechanisms of secondary nucleation in agitated crystallizers. AIChE J. 20, 950–958. http://dx.doi.org/10.1002/aic.690200516.

Evans, A.G., Suo, Z., Wang, R.Z., Aksay, I.A., He, M.Y., Hutchinson, J.W., 2001. Model for the robust mechanical behavior of nacre. J. Mater. Res. 16, 2475–2484. http://dx.doi.org/10.1557/JMR.2001.0339.

Falini, G., Albeck, S., Weiner, S., Addadi, L., 1996. Control of aragonite or calcite polymorphism by mollusk shell macromolecules. Science 271, 67–69.

Fantner, G.E., Hassenkam, T., Kindt, J.H., Weaver, J.C., Birkedal, H., Pechenik, L., Cutroni, J.A., Cidade, G.A.G., Stucky, G.D., Morse, D.E., Hansma, P.K., 2005. Sacrificial bonds and hidden length dissipate energy as mineralized fibrils separate during bone fracture. Nat. Mater. 4, 612–616. http://dx.doi.org/10.1038/nmat1428.

Ford, I.J., Laaksonen, A., Kulmala, M., 1993. Modification of the Dillmann-Meier theory of homogeneous nucleation. J. Chem. Phys. 99, 764. http://dx.doi.org/10.1063/1.465756.

Gago-Duport, L., Briones, M.J.I., Rodríguez, J.B., Covelo, B., 2008. Amorphous calcium carbonate biomineralization in the earthworm's calciferous gland: pathways to the formation of crystalline phases. J. Struct. Biol. 162, 422–435. http://dx.doi.org/10.1016/j.jsb.2008.02.007.

Gal, A., Kahil, K., Vidavsky, N., DeVol, R.T., Gilbert, P.U.P.A., Fratzl, P., Weiner, S., Addadi, L., 2014. Particle accretion mechanism underlies biological crystal growth from an amorphous precursor phase. Adv. Funct. Mater. 24, 5420–5426. http://dx.doi.org/10.1002/adfm.201400676.

Gal, A., Weiner, S., Addadi, L., 2015. A perspective on underlying crystal growth mechanisms in biomineralization: solution mediated growth versus nanosphere particle accretion. CrystEngComm 17, 2606–2615. http://dx.doi.org/10.1039/C4CE01474J.

Gao, H., Ji, B., Jager, I.L., Arzt, E., Fratzl, P., 2003. Materials become insensitive to flaws at nanoscale: lessons from nature. Proc. Nat. Acad. Sci. USA 100, 5597–5600. http://dx.doi.org/10.1073/pnas.0631609100.

Garant, P.R., Nalbandian, J., 1968. Observations on the ultrastructure of ameloblasts with special reference to the Golgi complex and related components. J. Ultrastruct. Res. 23, 427–443. http://dx.doi.org/10.1016/S0022-5320(68)80108-X.

Gilis, M., Grauby, O., Willenz, P., Dubois, P., Legras, L., Heresanu, V., Baronnet, A., 2011. Multi-scale mineralogical characterization of the hypercalcified sponge *Petrobiona massiliana* (Calcarea, Calcaronea). J. Struct. Biol. 176, 315–329. http://dx.doi.org/10.1016/j.jsb.2011.08.008.

Gong, Y.U.T., Killian, C.E., Olson, I.C., Appathurai, N.P., Amasino, A.L., Martin, M.C., Holt, L.J., Wilt, F.H., Gilbert, P.U.P.A., 2012. Phase transitions in biogenic amorphous calcium carbonate. Proc. Nat. Acad. Sci. USA 1–6. http://dx.doi.org/10.1073/pnas.1118085109.

Gordon, L.M., Cohen, M.J., MacRenaris, K.W., Pasteris, J.D., Seda, T., Joester, D., Ferences, R.E., 2015. Amorphous intergranular phases control the properties of rodent tooth enamel. Science 347, 746–750. http://dx.doi.org/10.1126/science.1258950.

Gower, L.B., 2008. Biomimetic model systems for investigating the amorphous precursor pathway and its role in biomineralization. Chem. Rev. 108, 4551–4627. http://dx.doi.org/10.1021/cr800443h.

Gower, L.B., Odom, D., 2000. Deposition of calcium carbonate films by a polymer-induced liquid-precursor (PILP) process. J. Cryst. Growth 210, 719–734. http://dx.doi.org/10.1016/S0022-0248(99)00749-6.

Gower, L.B., Tirrell, D.A., 1998. Calcium carbonate films and helices grown in solutions of poly(aspartate). J. Cryst. Growth 191, 153–160. http://dx.doi.org/10.1016/S0022-0248(98)00002-5.

Griffith, A.A., 1921. The phenomena of rupture and flow in solids. Philos. Trans. A 221, 163–198.

Habelitz, S., Marshall Jr, S.J., G.W.M., Balooch, M., 2001. Mechanical properties of human dental enamel on the nanometre scale. Arch. Oral Biol. 46, 173–183. http://dx.doi.org/10.1016/S0003-9969(00)00089-3.

Harrington, M.J., Masic, A., Holten-Andersen, N., Waite, J.H., Fratzl, P., 2010. Iron-clad fibers: a metal-based biological strategy for hard flexible coatings. Science 328, 216–220. http://dx.doi.org/10.1126/science.1181044.

Harris, J., Mey, I., Hajir, M., Mondeshki, M., Wolf, S.E., 2015. Pseudomorphic transformation of amorphous calcium carbonate films follows spherulitic growth mechanisms and can give rise to crystal lattice tilting. CrystEngComm 17, 6831–6837. http://dx.doi.org/10.1039/C5CE00441A.

Hasse, B., Ehrenberg, H., Marxen, J.C., Becker, W., Epple, M., 2000. Calcium carbonate modifications in the mineralized shell of the freshwater snail *Biomphalaria glabrata*. Chem. Eur. J. 6, 3679–3685.

He, G., Dahl, T., Veis, A., George, A., 2003. Nucleation of apatite crystals in vitro by self-assembled dentin matrix protein 1. Nat. Mater. 2, 552–558. http://dx.doi.org/10.1038/nmat945.

Helmholtz, R. von, 1886. Investigations of vapors and mists, especially of such things from solutions. Ann. Phys. 263, 508–543.

Hench, L.L., 1991. Bioceramics: From Concept to Clinic. J. Am. Ceram. Soc. 74, 1487–1510. http://dx.doi.org/10.1111/j.1151-2916.1991.tb07132.x.

Hench, L.L., Thompson, I., 2010. Twenty-first century challenges for biomaterials. J. R. Soc. Interface 7, S379–S391. http://dx.doi.org/10.1098/rsif.2010.0151.focus.

Henriksen, K., Stipp, S.L.S., Young, J.R., Bown, P.R., 2003. Tailoring calcite: nanoscale AFM of coccolith biocrystals. Am. Mineral. 88, 2040–2044.

Henriksen, K., Young, J., Bown, P., Stipp, S.L.S., 2004. Coccolith biomineralisation studied with atomic force microscopy. Palaeontology 47, 725–743. http://dx.doi.org/10.1111/j.0031-0239.2004.00385.x.

Herman, M.A., Richter, W., Sitter, H., 2004. Epitaxy: Physical Principles and Technical Implementation, Series. Springer, New York.

Homeijer, S.J., Barrett, R.A., Gower, L.B., 2010. Polymer-Induced Liquid-Precursor (PILP) Process in the Non-Calcium Based Systems of Barium and Strontium Carbonate. Cryst. Growth Des. 10, 1040–1052. http://dx.doi.org/10.1021/cg800918g.

Hovden, R., Wolf, S.E., Holtz, M.E., Marin, F., Muller, D.A., Estroff, L.A., 2015. Nanoscale assembly processes revealed in the. Nat. Commun. 6, 10097. http://dx.doi.org/10.1038/ncomms10097.

Huang, Z., Li, X., 2012. Order-disorder transition of aragonite nanoparticles in nacre. Phys. Rev. Lett. 109, 1–5. http://dx.doi.org/10.1103/PhysRevLett. 109.025501.

Huang, Z., Li, X., 2013. Origin of flaw-tolerance in nacre. Sci. Rep. 3, 1693. http://dx.doi.org/10.1038/srep01693.

Isa, Y., 1986. An electron microscope study on the mineralization of the skeleton of the staghorn coral Acropora hebes. Mar Biol 93, 91–101. http://dx.doi.org/10.1007/BF00428658.

Jacob, D.E., Soldati, A., Wirth, R., Huth, J., Wehrmeister, U., Hofmeister, W., 2008. Nanostructure, composition and mechanisms of bivalve shell growth. Geochim. Cosmochim. Acta 72, 5401–5415. http://dx.doi.org/10.1016/j.gca.2008.08.019.

Jacob, D.E., Wirth, R., Soldati, A., Wehrmeister, U., Schreiber, A., 2011. Amorphous calcium carbonate in the shells of adult Unionoida. J. Struct. Biol. 173, 241–249. http://dx.doi.org/10.1016/j.jsb.2010.09.011.

Joubert, C., Piquemal, D., Marie, B., Manchon, L., Pierrat, F., Zanella-Cléon, I., Cochennec-Laureau, N., Gueguen, Y., Montagnani, C., 2010. Transcriptome and proteome analysis of *Pinctada margaritifera* calcifying mantle and shell: focus on biomineralization. BMC Genomics 11, 613. http://dx.doi.org/10.1186/1471-2164-11-613.

Kallenbach, E., 1971. Electron microscopy of the differentiating rat incisor ameloblast. J. Ultrasruct. Res. 35, 508–531. http://dx.doi.org/10.1016/S0022-5320(71)80008-4.

Kane, S.G., Evans, T.W., Brian, P.L.T., Sarofim, A.F., 1974. Determination of the kinetics of secondary nucleation in batch crystallizers. AIChE J. 20, 855–862. http://dx.doi.org/10.1002/aic.690200505.

Kerschnitzki, M., Akiva, A., Shoham, A..Ben., Koifman, N., Shimoni, E., Rechav, K., Arraf, A.A., Schultheiss, T.M., Talmon, Y., Zelzer, E., Weiner, S., Addadi, L., 2016. Transport of membrane-bound mineral particles in blood vessels during chicken embryonic bone development. Bone 83, 65–72. http://dx.doi.org/10.1016/j.bone.2015.10.009.

Killian, C.E., Metzler, R., Gong, Y.U.T., Olson, I.C., Aizenberg, J., Politi, Y., Wilt, F.H., Scholl, A., Young, A., Doran, A., Kunz, M., Tamura, N., Coppersmith, S.N., Gilbert, P.U.P.A., 2009. Mechanism of calcite co-orientation in the sea urchin tooth. J. Am. Chem. Soc. 131, 18404–18409. http://dx.doi.org/10.1021/ja907063z.

Kim, S., Inoue, S., Akisaka, T., 1994. Ultrastructure of quick-frozen secretory ameloblasts of the rat molar tooth. Tissue Cell 26, 29–41. http://dx.doi.org/10.1016/0040-8166(94)90081-7.

Kim, W., Choi, H.C., Shim, M., Li, Y., Wang, D., Dai, H., 2002. Synthesis of ultralong and high percentage of semiconducting single-walled carbon nanotubes. Nano Lett. 2, 703–708. http://dx.doi.org/10.1021/nl025602q.

Kim, Y.-Y., Douglas, E.P., Gower, L.B., Science, M., Uni, V., Hall, R., Box, P.O., Gaines, V., 2007. Patterning Inorganic $CaCO_3$ Thin Films via a Polymer-Induced Liquid-Precursor Process. Langmuir 151, 4862–4870.

Kirkland, B.L., Leo Lynch, F., Rahnis, M.A., Folk, R.L., Molineux, I.J., McLean, R.J.C., 1999. Alternative origins for nannobacteria-like objects in calcite. Geology 27, 347. http://dx.doi.org/10.1130/0091-7613(1999) 027.

Kopp, C., Meibom, A., Beyssac, O., Stolarski, J., Djediat, S., Szlachetko, J., Domart-Coulon, I., 2011. Calcareous sponge biomineralization: ultrastructural and compositional heterogeneity of spicules in Leuconia johnstoni. J. Struct. Biol. 173, 99–109. http://dx.doi.org/10.1016/j.jsb.2010.07.006.

Lemloh, M., 2015. Biomineralization in ciliates. Key Eng. Mater. 672, 40–46. http://dx.doi.org/10.4028/www.scientific.net/KEM.672.40.

Levi-Kalisman, Y., Albeck, S., Brack, A., Weiner, S., Addadi, L., 1998. Control over aragonite crystal nucleation and growth: an in vitro study of biomineralization. Chem. Eur. J. 4, 389–396. http://dx.doi.org/10.1002/(SICI)1521-3765(19980310)4:3<389::AID-CHEM389>3.0.CO;2-X.

Li, L., Ortiz, C., 2013. Biological design for simultaneous optical transparency and mechanical robustness in the shell of *Placuna placenta*. Adv. Mater. 25, 2344–2350. http://dx.doi.org/10.1002/adma.201204589.

Li, L., Ortiz, C., 2014. Pervasive nanoscale deformation twinning as a catalyst for efficient energy dissipation in a bioceramic armour. Nat. Mater. 13, 501–507. http://dx.doi.org/10.1038/nmat3920.

Li, X., Chang, W.-C., Chao, Y.J., Wang, R., Chang, M., 2004. Nanoscale structural and mechanical characterization of a natural nanocomposite material: the shell of red abalone. Nano Lett. 4, 613–617. http://dx.doi.org/10.1021/nl049962k.

Li, X., Xu, Z.-H., Wang, R., 2006a. In situ observation of nanograin rotation and deformation in nacre. Nano Lett. 6, 2301–2304. http://dx.doi.org/10.1021/nl061775u.

Li, X., Xu, Z.-H., Wang, R., 2006b. In situ observation of nanograin rotation and deformation in nacre. Nano Lett. 6, 2301–2304. http://dx.doi.org/10.1021/nl061775u.

Li, D., Nielsen, M.H., Lee, J.R.I., Frandsen, C., Banfield, J.F., De Yoreo, J.J., 2012. Direction-specific interactions control crystal growth by oriented attachment. Science 336, 1014–1018. http://dx.doi.org/10.1126/science.1219643.

Loste, E., Park, R.J., Warren, J., Meldrum, F.C., 2004. Precipitation of Calcium Carbonate in Confinement. Adv. Funct. Mater. 14, 1211–1220. http://dx.doi.org/10.1002/adfm.200400268.

Lyons Ryall, R., Fleming, D.E., Doyle, I.R., Evans, N.A., Dean, C.J., Marshall, V.R., 2001. Intracrystalline proteins and the hidden ultrastructure of calcium oxalate urinary crystals: implications for kidney stone formation. J. Struct. Biol. 134, 5–14. http://dx.doi.org/10.1006/jsbi.2001.4363.

Magonov, S.N., Elings, V., Whangbo, M.-H., 1997. Phase imaging and stiffness in tapping-mode atomic force microscopy. Surf. Sci. 375, L385–L391. http://dx.doi.org/10.1016/S0039-6028(96)01591-9.

Mahamid, J., Sharir, A., Addadi, L., Weiner, S., 2008. Amorphous calcium phosphate is a major component of the forming fin bones of zebrafish: Indications for an amorphous precursor phase. Proc. Nat. Acad. Sci. USA 105, 12748–12753. http://dx.doi.org/10.1073/pnas.0803354105.

Mahamid, J., Sharir, A., Gur, D., Zelzer, E., Addadi, L., Weiner, S., 2011. Bone mineralization proceeds through intracellular calcium phosphate loaded vesicles: a cryo-electron microscopy study. J. Struct. Biol. 174, 527–535. http://dx.doi.org/10.1016/j.jsb.2011.03.014.

Margolin, L., 1984. A generalized Griffith criterion for crack propagation. Engin. Fract. Mech. 19, 539–543. http://dx.doi.org/10.1016/0013-7944(84)90010-9.

Marie, B., Joubert, C., Tayalé, A., Zanella-Cléon, I., Belliard, C., Piquemal, D., Cochennec-Laureau, N., Marin, F., Gueguen, Y., Montagnani, C., 2012. Different secretory repertoires control the biomineralization processes of prism and nacre deposition of the pearl oyster shell. Proc. Nat. Acad. Sci. USA 109, 20986–20991. http://dx.doi.org/10.1073/pnas.1210552109.

Marin, F., Luquet, G., 2007. Unusually Acidic Proteins in Biomineralization. In: Handbook of Biomineralization: Biological Aspects and Structure Formation. Wiley-VCH Verlag GmbH, Weinheim, Germany. http://dx.doi.org/10.1002/9783527619443.ch16.

Marin, F., Marie, B., Hamada, S. .Ben., Silva, P., Roy, N. .Le., Wolf, S.E., Montagnani, C., Joubert, C., Piquemal, D., 2013. "Shellome": proteins involved in mollusc shell biomineralization – diversity, functions. In: Watabe, S., Maeyama, K., Nagasawa, H. (Eds.), Recent Advances in Pearl Research. Terrapub, pp. 149–166.

Marin, F., Roy, N..Le., Marie, B., Ramos-Silva, P., Wolf, S.E., Benhamada, S., Guichard, N., Immel, F., Le Roy, N., 2014. Synthesis of calcium carbonate biological materials : how many proteins are needed? Key Eng. Mater. 614, 52–61. http://dx.doi.org/10.4028/www.scientific.net/KEM.614.52.

McCabe, W., Smith, J., Harriott, P., 2004. Unit Operations of Chemical Engineering, 7th ed. McGraw-Hill, New York.

McLean, R.S., Sauer, B.B., 1997. Tapping-mode AFM studies using phase detection for resolution of nanophases in segmented polyurethanes and other block copolymers. Macromolecules 30, 8314–8317. http://dx.doi.org/10.1021/ma970350e.

Meldrum, F.C., Cölfen, H., 2008. Controlling mineral morphologies and structures in biological and synthetic systems. Chem. Rev. 108, 4332–4432. http://dx.doi.org/10.1021/cr8002856.

Mohanty, B., Katti, K.S., Katti, D.R., Verma, D., 2011. Dynamic nanomechanical response of nacre. J. Mater. Res. 21, 2045–2051. http://dx.doi.org/10.1557/jmr.2006.0247.

Montagnani, C., Marie, B., Marin, F., Belliard, C., Riquet, F., Tayalé, A., Zanella-Cléon, I., Fleury, E., Gueguen, Y., Piquemal, D., Cochennec-Laureau, N., 2011. Pmarg-pearlin is a matrix protein involved in nacre framework formation in the pearl oyster Pinctada margaritifera. ChemBioChem 12, 2033–2043. http://dx.doi.org/10.1002/cbic.201100216.

Müller, W.E.G., Wolf, S.E., Schlossmacher, U., Wang, X.-H., Boreiko, A., Brandt, D., Tremel, W., Schröder, H.-C., 2008. Poly(silicate)-metabolizing silicatein in siliceous spicules and silicasomes of demosponges comprises dual enzymatic activities (silica polymerase and silica esterase). FEBS J. 275, 362–370. http://dx.doi.org/10.1111/j.1742-4658.2007.06206.x.

Mutvei, H., 1972. Ultrastructural studies on cephalopod shells. Part 1: The septa and siphonal tube in Nautilus. Bull. Geol. Institutions Univ. Uppsala 3, 237–261. http://dx.doi.org/10.1017/CBO9781107415324.004.

Mutvei, H., Dunca, E., 2008. Structural relationship between interlamellar organic sheets and nacreous tablets in gastropods and the cephalopod Nautilus. Paläontologische Zeitschrift 82, 85–94. http://dx.doi.org/10.1007/BF02988434.

Mutvei, H., Dunca, E., 2010. Crystalline structure, orientation and nucleation of the nacreous tablets in the cephalopod Nautilus. Paläontologische Zeitschrift 84, 457–465. http://dx.doi.org/10.1007/s12542-010-0060-2.

Nassif, N., Pinna, N., Gehrke, N., Antonietti, M., Jäger, C., Cölfen, H., 2005. Amorphous layer around aragonite platelets in nacre. Proc. Nat. Acad. Sci. U.S.A. 102, 12653–12655. http://dx.doi.org/10.1073/pnas.0502577102.

Neff, J.M., 1972. Ultrastructural studies of Periostracum formation in the hard shelled clam Mercenaria mercenaria (L). Tissue Cell 4, 311–326. http://dx.doi.org/10.1016/S0040-8166(72)80050-8.

Nouet, J., Baronnet, A., Howard, L., 2012. Crystallization in organo-mineral micro-domains in the crossed-lamellar layer of *Nerita undata* (Gastropoda, Neritopsina). Micron 43, 456–462. http://dx.doi.org/10.1016/j.micron.2011.10.027.

Nudelman, F., Chen, H.H., Goldberg, H.A., Weiner, S., Addadi, L., 2007. Spiers memorial lecture: lessons from biomineralization: comparing the growth strategies of mollusc shell prismatic and nacreous layers in *Atrina rigida*. Faraday Disc. 136, 9–25. http://dx.doi.org/10.1039/b704418f.

Nudelman, F., Sonmezler, E., Bomans, P.H.H., de With, G., Sommerdijk, N.A.J.M., 2010. Stabilization of amorphous calcium carbonate by controlling its particle size. Nanoscale 2, 2436–2439. http://dx.doi.org/10.1039/c0nr00432d.

Oaki, Y., Imai, H., 2005. The hierarchical architecture of nacre and its mimetic material. Angew. Chem. 117, 6729–6733. http://dx.doi.org/10.1002/ange.200500338.

Oaki, Y., Imai, H., 2006. Nanoengineering in echinoderms: the emergence of morphology from nanobricks. Small 2, 66–70. http://dx.doi.org/10.1002/smll.200500246.

Ohnesorge, F., Binnig, G., 1993. True atomic resolution by atomic force microscopy through repulsive and attractive forces. Science 260, 1451–1456.

Okumura, T., Suzuki, M., Nagasawa, H., Kogure, T., 2012. Microstructural variation of biogenic calcite with intracrystalline organic macromolecules. Cryst. Growth Des. 12, 224–230. http://dx.doi.org/10.1021/cg200947c.

Olson, I.C., Metzler, R., Tamura, N., Kunz, M., Killian, C.E., Gilbert, P.U.P.A., 2013. Crystal lattice tilting in prismatic calcite. J. Struct. Biol. 183, 180–190. http://dx.doi.org/10.1016/j.jsb.2013.06.006.

Orme, C., Noy, A., Wierzbicki, A., McBride, M.T., Grantham, M., Teng, H.H., Dove, P.M., De Yoreo, J.J., 2001. Formation of chiral morphologies through selective binding of amino acids to calcite surface steps. Nature 411, 775–779. http://dx.doi.org/10.1038/35081034.

Penn, R.L., 1998. Imperfect oriented attachment: dislocation generation in defect-free nanocrystals. Science 281, 969–971. http://dx.doi.org/10.1126/science.281.5379.969.

Penn, R.L., Banfield, J.F., 1998. Oriented attachment and growth, twinning, polytypism, and formation of metastable phases: Insights from nanocrystalline TiO2. Am. Miner. 83, 1077–1082.

Penn, R.L., Soltis, J.A., 2014. Characterizing crystal growth by oriented aggregation. CrystEngComm 16, 1409. http://dx.doi.org/10.1039/c3ce41773e.

Perez, M., 2005. Gibbs-Thomson effects in phase transformations. Scr. Mater. 52, 709–712. http://dx.doi.org/10.1016/j.scriptamat.2004.12.026.

Perez-Huerta, A., Dauphin, Y., Cusack, M., 2013. Biogenic calcite granules-Are brachiopods different? Micron 44, 395–403. http://dx.doi.org/10.1016/j.micron.2012.09.005.

Politi, Y., Levi-Kalisman, Y., Raz, S., Wilt, F.H., Addadi, L., Weiner, S., Sagi, I., 2006. Structural characterization of the transient amorphous calcium carbonate precursor phase in sea urchin embryos. Adv. Funct. Mater. 16, 1289–1298. http://dx.doi.org/10.1002/adfm.200600134.

Politi, Y., Metzler, R.A., Abrecht, M., Gilbert, B., Wilt, F.H., Sagi, I., Addadi, L., Weiner, S., Gilbert, P.U.P.A., 2008. Transformation mechanism of amorphous calcium carbonate into calcite in the sea urchin larval spicule. Proc. Nat. Acad. Sci. U.S.A. 105, 17362–17366. http://dx.doi.org/10.1073/pnas.0806604105.

Reith, E.J., 1967. The early stage of amelogenesis as observed in molar teeth of young rats. J. Ultrasruct. Res. 17, 503–526.

Rodríguez-Navarro, A.B., Marie, P., Nys, Y., Hincke, M.T., Gautron, J., 2015. Amorphous calcium carbonate controls avian eggshell mineralization: a new paradigm for understanding rapid eggshell calcification. J. Struct. Biol. 190, 291–303.

Rodriguez-Navarro, C., Ruiz-Agudo, E., Harris, J., Wolf, S.E., 2016. Nonclassical crystallization in vivo et in vitro (II): nanogranular features in biomimetic minerals disclose a general colloid-mediated crystal growth mechanism. J. Struct. Biol.

Rohde, M., Mayer, H., 2007. Exocytotic process as a novel model for mineralization by osteoblasts in vitro and in vivo determined by electron microscopic analysis. Calcif. Tissue Int. 80, 323–336. http://dx.doi.org/10.1007/s00223-007-9013-5.

Rousseau, M., Lopez, E., Stempflé, P., Brendlé, M., Franke, L., Guette, A., Naslain, R., Bourrat, X., 2005. Multiscale structure of sheet nacre. Biomaterials 26, 6254–6262. http://dx.doi.org/10.1016/j.biomaterials.2005.03.028.

Sandersius, S., Rez, P., 2007a. Morphology of crystals in calcium oxalate monohydrate kidney stones. Urol. Res. 35, 287–293. http://dx.doi.org/10.1007/s00240-007-0115-3.

Sandersius, S., Rez, P., 2007b. Morphology of crystals in calcium oxalate monohydrate kidney stones. Urol. Res. 35, 287–293. http://dx.doi.org/10.1007/s00240-007-0115-3.

Sethmann, I., 2005. Observation of nano-clustered calcite growth via a transient phase mediated by organic polyanions: a close match for biomineralization. Am. Miner. 90, 1213–1217. http://dx.doi.org/10.2138/am.2005.1833.

Sethmann, I., Hinrichs, R., Wörheide, G., Putnis, A., 2006. Nano-cluster composite structure of calcitic sponge spicules–a case study of basic characteristics of biominerals. J. Inorg. Biochem. 100, 88–96. http://dx.doi.org/10.1016/j.jinorgbio.2005.10.005.

Seto, J., Ma, Y., Davis, S.A., Meldrum, F.C., Gourrier, A., Kim, Y.-Y., Schilde, U., Sztucki, M., Burghammer, M., Maltsev, S., Jäger, C., Cölfen, H., 2012. Structure-property relationships of a biological mesocrystal in the adult sea urchin spines. Proc. Nat. Acad. Sci. USA 109, 1–6. http://dx.doi.org/10.1073/pnas.1109243109.

Smith, B.L., Schaffer, T.E., Viani, M., Thompson, J.B., Frederick, N.A., Kindt, J., Belcher, A.M., Stucky, G.D., Morse, D.E., Hansma, P.K., 1999. Molecular mechanistic origin of the toughness of natural adhesives, fibres and composites. Nature 399, 761–763. http://dx.doi.org/10.1038/21607.

Stempflé, P., Brendlé, M., 2006. Tribological behaviour of nacre—Influence of the environment on the elementary wear processes. Tribol. Int. 39, 1485–1496. http://dx.doi.org/10.1016/j.triboint.2006.01.011.

Stephens, C.J., Ladden, S.F., Meldrum, F.C., Christenson, H.K., 2010. Amorphous calcium carbonate is stabilized in confinement. Adv. Funct. Mater. 20, 2108–2115. http://dx.doi.org/10.1002/adfm.201000248.

Stipp, S.L.S., Eggleston, C.M., Nielsen, B.S., 1994. Calcite surface structure observed at microtopographic and molecular scales with atomic force microscopy (AFM). Geochim. Cosmochim. Acta 58, 3023–3033. http://dx.doi.org/10.1016/0016-7037(94)90176-7.

Stolarski, J., 2003. Three-dimensional and nanostructural characteristics of the scleractinian corals skeleton: a biocalcification proxy. Acta Palaeo. Pol. 48, 497–530.

Stolarski, J., Mazur, M., 2005. Nanostructure of biogenic versus abiogenic calcium carbonate crystals. Acta Palaeo. Pol. 50, 847–865. http://dx.doi.org/10.1029/2004GC000783.

Stolarski, J., Meibom, A., Przenioslo, R., Mazur, M., 2007. A Cretaceous scleractinian coral with a calcitic skeleton. Science 318, 92–94. http://dx.doi.org/10.1126/science.1149237.

Stolarski, J., Gorzelak, P., Mazur, M., Marrocchi, Y., Meibom, A., 2009. Nanostructural and geochemical features of the jurassic isocrinid columnal ossicles. Acta Palaeo. Pol. 54, 69–75. http://dx.doi.org/10.4202/app.2009.0108.

Sumitomo, T., Kakisawa, H., Owaki, Y., Kagawa, Y., 2008. Transmission electron microscopy observation of nanoscale deformation structures in nacre. J. Mater. Res. 23, 3213–3221. http://dx.doi.org/10.1557/jmr.2008.0389.

Sundar, V.C., Yablon, A.D., Grazul, J.L., Ilan, M., Aizenberg, J., 2003. Fibre-optical features of a glass sponge. Nature 424, 899–900. http://dx.doi.org/10.1038/424899a.

Suzuki, M., Okumura, T., Nagasawa, H., Kogure, T., 2011. Localization of intracrystalline organic macromolecules in mollusk shells. J. Cryst. Growth 337, 24–29. http://dx.doi.org/10.1016/j.jcrysgro.2011.10.013.

Sviben, S., Gal, A., Hood, M.A., Bertinetti, L., Politi, Y., Bennet, M., Krishnamoorthy, P., Schertel, A., Wirth, R., Sorrentino, A., Pereiro, E., Faivre, D., Scheffel, A., 2016. A vacuole-like compartment concentrates a disordered calcium phase in a key coccolithophorid alga. Nat. Commun. 7, 11228. http://dx.doi.org/10.1038/ncomms11228.

Tai, K., Ulm, F.J., Ortiz, C., 2006. Nanogranular origins of the strength of bone. Nano Lett. 6, 2520–2525. http://dx.doi.org/10.1021/nl061877k.

Takahashi, K., Yamamoto, H., Onoda, A., Doi, M., Inaba, T., Chiba, M., Kobayashi, A., Taguchi, T., Okamura, T., Ueyama, N., 2004. Highly oriented aragonite nanocrystal-biopolymer composites in an aragonite brick of the nacreous layer of *Pinctada fucata*. Chem. Commun. 6, 996–997. http://dx.doi.org/10.1039/b315478e.

Tang, R., Wang, L., Orme, C.A., Bonstein, T., Bush, P.J., Nancollas, G.H., 2004. Dissolution at the nanoscale: self-preservation of biominerals. Angew. Chem. Int. Ed. 43, 2697–2701. http://dx.doi.org/10.1002/anie.200353652.

Tavare, N.S., 1995. Industrial Crystallization. Plenum Press, New York.

Taylor, J.D., 1964. The structural evolution of the bivalve shell. Palaeontology 7, 220–239.

Taylor, J.D., Kennedy, W.J., Hall, A., 1969. The shell structure and mineralogy of the Bivalvia. Nuculacea—Trigonacea. Bull. Brit. Mus. Suppl. 3, 1–125.

Thompson, J.B., Kindt, J.H., Drake, B., Hansma, H.G., Morse, D.E., Hansma, P.K., 2001. Bone indentation recovery time correlates with bond reforming time. Nature 414, 773–776. http://dx.doi.org/10.1038/414773a.

Tolman, R.C., 1948. Consideration of the Gibbs theory of surface tension. J. Chem. Phys. 16, 758. http://dx.doi.org/10.1063/1.1746994.

Tolman, R.C., 1949. The effect of droplet size on surface tension. J. Chem. Phys. 17, 333. http://dx.doi.org/10.1063/1.1747247.

Towe, K.M., Lowenstam, H.A., 1967. Ultrastructure and development of iron mineralization in the radular teeth of *Cryptochiton stelleri* (mollusca). J. Ultrastruct. Res. 17, 1–13. http://dx.doi.org/10.1016/S0022-5320(67)80015-7.

Vielzeuf, D., Garrabou, J., Baronnet, A., Grauby, O., Marschal, C., 2008. Nano to macroscale biomineral architecture of red coral (Corallium rubrum). Am. Mineral. 93, 1799–1815. http://dx.doi.org/10.2138/am.2008.2923.

Vielzeuf, D., Floquet, N., Chatain, D., Bonneté, F., Ferry, D., Garrabou, J., Stolper, E.M., 2010. Multilevel modular mesocrystalline organization in red coral. Am. Mineral. 95, 242–248, doi:2138/am.2010.3268.

Wang, R.Z., Suo, Z., Evans, A.G., Yao, N., Aksay, I.A., 2001. Deformation mechanisms in nacre. J. Mater. Res. 16, 2485–2493. http://dx.doi.org/10.1557/JMR.2001.0340.

Wang, T., Cölfen, H., Antonietti, M., 2005. Nonclassical crystallization: Mesocrystals and morphology change of $CaCO_3$ crystals in the presence of a polyelectrolyte additive. J. Am. Chem. Soc. 127, 3246–3247. http://dx.doi.org/10.1021/ja045331g.

Wang, T., Antonietti, M., Cölfen, H., 2006. Calcite Mesocrystals: ‘‘Morphing” Crystals by a Polyelectrolyte. Chem. -Eur. J. 12, 5722–5730. http://dx.doi.org/10.1002/chem.200501019.

Wang, Y.-W., Christenson, H.K., Meldrum, F.C., 2013. Confinement Leads to Control over Calcium Sulfate Polymorph. Adv. Funct. Mater. 23, 5615–5623. http://dx.doi.org/10.1002/adfm.201300861.

Watabe, N., 1983. Shell repair. In: Wilbur, K.M., Saleuuddin, A. (Eds.), The Mollusca, Physiology, Part 1, vol. 4. Academic Press, Inc (London) LTD, New York, pp. 289–310.

Watabe, N., Meenakshi, V.R., Blackwelder, P.L., Kurtz, E.M., Dunkelberger, D.G., 1976. Mechanisms of Biomineralization in the Invertebrates and Plants. University South Carolina Press, Columbia.

Weaver, J.C., Pietrasanta, L.I., Hedin, N., Chmelka, B.F., Hansma, P.K., Morse, D.E., 2003. Nanostructural features of demosponge biosilica. J. Struct. Biol. 144, 271–281. http://dx.doi.org/10.1016/j.jsb.2003.09.031.

Weaver, J.C., Aizenberg, J., Fantner, G.E., Kisailus, D., Woesz, A., Allen, P., Fields, K., Porter, M.J., Zok, F.W., Hansma, P.K., Fratzl, P., Morse, D.E., 2007. Hierarchical assembly of the siliceous skeletal lattice of the hexactinellid sponge *Euplectella aspergillum*. J. Struct. Biol. 158, 93–106. http://dx.doi.org/10.1016/j.jsb.2006.10.027.

Wegst, U.G.K., Bai, H., Saiz, E., Tomsia, A.P., Ritchie, R.O., 2014. Bioinspired structural materials. Nat. Mater. 14, 23–36. http://dx.doi.org/10.1038/nmat4089.

Weiner, S., Addadi, L., 1997. Design strategies in mineralized biological materials. J. Mater. Chem. 7, 689–702. http://dx.doi.org/10.1039/a604512j.

Weiner, S., Addadi, L., 2011. Crystallization pathways in biomineralization. Annu. Rev. Mater. Res. 41, 21–40. http://dx.doi.org/10.1146/annurev-matsci-062910-095803.

Weiner, S., Sagi, I., Addadi, L., 2005. Choosing the crystallization path less traveled. Science 309, 1027–1028. http://dx.doi.org/10.1126/science.1114920.

Wolf, S.E., Gower, L.B., 2016. Challenges and perspectives of the polymer-induced liquid-precursor process: the pathway from liquid-condensed mineral precursors to mesocrystalline products. In: Kellermeier, M., van Driessche, A., Benning, L., Gebauer, D. (Eds.), New Perspectives on Mineral Nucleation and Growth. Springer.

Wolf, S.E., Leiterer, J., Kappl, M., Emmerling, F., Tremel, W., 2008. Early homogenous amorphous precursor stages of calcium carbonate and subsequent crystal growth in levitated droplets. J. Am. Chem. Soc. 130, 12342–12347. http://dx.doi.org/10.1021/ja800984y.

Wolf, S.E., Leiterer, J., Pipich, V., Barrea, R., Emmerling, F., Tremel, W., 2011a. Strong stabilization of amorphous calcium carbonate emulsion by ovalbumin: gaining insight into the mechanism of ‘‘polymer-induced liquid precursor” processes. J. Am. Chem. Soc. 133, 12642–12649. http://dx.doi.org/10.1021/ja202622g.

Wolf, S.E., Müller, L., Barrea, R., Kampf, C.J., Leiterer, J., Panne, U., Hoffmann, T., Emmerling, F., Tremel, W., 2011b. Carbonate-coordinated metal complexes precede the formation of liquid amorphous mineral emulsions of divalent metal carbonates. Nanoscale 3, 1158–1165. http://dx.doi.org/10.1039/c0nr00761g.

Wolf, S.E., Lieberwirth, I., Natalio, F., Bardeau, J.-F., Delorme, N., Emmerling, F., Barrea, R., Kappl, M., Marin, F., 2012. Merging models of biomineralisation with concepts of nonclassical crystallisation: is a liquid amorphous precursor involved in the formation of the prismatic layer of the Mediterranean Fan Mussel Pinna nobilis? Faraday Discuss. 159, 433. http://dx.doi.org/10.1039/c2fd20045g.

Wolf, S.E., Böhm, C., Harris, J., Hajir, M., Mondeshki, M., Marin, F., 2015. Single nanogranules preserve intracrystalline amorphicity in biominerals. Key Eng. Mater. 672, 47–59. http://dx.doi.org/10.4028/www.scientific.net/KEM.672.47.

Wolf, S.E., Harris, J., Lovett, A., Gower, L.B., 2016. Non-classical crystallization processes: potential relevance to stone formation. In: Coe, F.L., Worcester, E.M., Lingeman, J.E., Evan, A.P. (Eds.), Kidney Stones: Medical and Surgical Management. Jaypee Medical Publishers, Philadelphia, PA.

Yang, L., Killian, C.E., Kunz, M., Tamura, N., Gilbert, P.U.P.A., 2011. Biomineral nanoparticles are space-filling. Nanoscale 3, 603–609. http://dx.doi.org/10.1039/c0nr00697a.

Younis, S., Kauffmann, Y., Bloch, L., Zolotoyabko, E., 2012. Inhomogeneity of nacre lamellae on the nanometer length scale. Cryst. Growth Des. 12, 4574–4579. http://dx.doi.org/10.1021/cg3007734.

Zhang, G., Xu, J., 2013. From colloidal nanoparticles to a single crystal: new insights into the formation of nacre's aragonite tablets. J. Struct. Biol. 182, 36–43. http://dx.doi.org/10.1016/j.jsb.2013.01.010.